

EVAPOTRANSPIRATION IN THE RIPARIAN ZONE OF THE LOWER BOISE RIVER
WITH IMPLICATIONS FOR GROUNDWATER FLOW

by

Brady Allen Johnson

A thesis

submitted in partial fulfillment

of the requirements for the degree of

Master of Science in Hydrologic Sciences

Boise State University

May 2011

© 2011

Brady Johnson

ALL RIGHTS RESERVED

BOISE STATE UNIVERSITY GRADUATE COLLEGE

DEFENSE COMMITTEE AND FINAL READING APPROVALS

of the thesis submitted by

Brady Allen Johnson

Thesis Title: Evapotranspiration in the Riparian Zone of the Lower Boise River with Implications for Groundwater Flow

Date of Final Oral Examination: 11 February 2011

The following individuals read and discussed the thesis submitted by student Brady Allen Johnson, and they evaluated his presentation and response to questions during the final oral examination. They found that the student passed the final oral examination.

Warren Barrash, Ph.D. Chair, Supervisory Committee

Bwalya Malama, Ph.D. Member, Supervisory Committee

Alejandro N. Flores, Ph.D. Member, Supervisory Committee

The final reading approval of the thesis was granted by Warren Barrash, Ph.D., Chair of the Supervisory Committee. The thesis was approved for the Graduate College by John R. Pelton, Ph.D., Dean of the Graduate College.

ACKNOWLEDGMENT

I am indebted to Dr. Warren Barrash for serving as the committee advisor to this thesis. The insight, time, and patience he provided was invaluable to the completion of the project. Many thanks to Dr. Bwalya Malama and Dr. Alejandro Flores for the outstanding input and direction in the crafting of this work. Special thanks to Mike Thoma for his assistance in data collection and providing supplemental site data.

Work presented in this thesis was supported by EPA under grants X-96004601-0 and X-96004601-1 and by the U.S. RDECOM ARL Army Research Office under grant W911NF-09-1-0534. Further support was provided by GSA through a graduate research grant.

ABSTRACT

Riparian zones in semi-arid regions often exhibit high rates of evapotranspiration (ET) in spite of low soil moisture content due to vegetation that is able to withdraw water from shallow aquifers. This work better defines the relationship between ET and the saturated zone by comparing the observed water table drawdown to analytically modeled drawdown in fully penetrating wells of an unconfined aquifer in response to daily ET flux. ET at the Boise Hydrogeophysical Research Site or BHRS (a riparian zone in a temperate, semi arid environment) is calculated following the approach of Batra *et al.* (2006) but uses site (or near site) measurements for air temperature and net radiation while relying on Landsat 5 data for quantification of vegetation. The resulting ET calculations represent a data set consisting of high resolution (30m x 30m) ET flux values obtained from minimal site measurements. Water table levels in the shallow, unconfined aquifer were monitored over the summer and fall of 2009 to record the timing and magnitude of daily fluctuations in four wells with different vegetation densities and distances from the nearby Boise River at the site. ET derived from the radiation-driven model of Batra *et al.* (2006) compares favorably with groundwater ET contribution rates calculated from well hydrographs (White, 1932), which further supports the finding of negligible water contribution coming from the unsaturated zone in shallow riparian aquifers in semi-arid regions (Shah *et al.*, 2007).

Using an analytical solution to ET induced drawdown (Malama & Johnson, 2010) for a semi-infinite (or river bounded) domain, daily drawdown is modeled in response to daily ET flux applied at the water table. Close agreement between observed and modeled drawdown supports the idea that ET can be estimated from well hydrographs in a well-characterized aquifer and conversely, if ET behavior is characterized, aquifer parameters like hydraulic conductivity and specific storage can be estimated from well hydrographs.

TABLE OF CONTENTS

ACKNOWLEDGMENT	iii
ABSTRACT	iv
LIST OF TABLES	viii
LIST OF FIGURES	ix
1 INTRODUCTION	1
1.1 Previous Work	2
1.2 Site Overview	3
1.3 Objectives	6
2 THEORY AND MODEL DEVELOPMENT	8
2.1 Transpiration	10
2.2 Phreatophytes and Diurnal Fluctuations of the Water Table	11
2.3 Evapotranspiration	12
2.4 Analytical Drawdown Model	15
3 METHODS	19
3.1 Characterization of Daily ET	20

3.2	Aquifer and River System Parameters	29
3.3	Well Monitoring	31
4	RESULTS	32
4.1	Daily Evapotranspiration	32
4.1.1	Seasonal Variation in ET signal	35
4.2	Daily Drawdown versus ET Magnitude across the Site	37
4.3	ET _g from White (1932)	41
4.4	Modeled Drawdown	41
5	DISCUSSION	47
5.1	Parameter Sensitivity Analysis	47
5.2	ET Parameter Correlation	51
5.3	Spatial Variation in ET Signal	51
5.4	Analytical Drawdown Model	54
6	SUMMARY AND CONCLUSIONS	57
	REFERENCES	59
	APPENDICES	64
A	ET AMPLITUDE FOR WELLS, 2009	64
B	FAO CALCULATIONS	72

LIST OF TABLES

1.1	Mean aquifer parameters resulting from analytical modeling of pumping tests (73 pumping well-observation well pairs) at the BHRS (Fox, 2006).	5
3.1	List of clear sky days with Landsat 5 TM images for the BHRS and calculated NDVI for four wells representing four different pixels.	25
3.2	Representative aquifer parameters derived from pumping tests (Barrash <i>et al.</i> , 2006; Fox, 2006) that are used for initial analytical drawdown model.	30
4.1	Average maximum and cumulative ET rates at four BHRS wells from May 18-September 1, 2009.	35
4.2	Distance from wells to the river July 3, 2009.	40
5.1	Results from parameter sensitivity simulation for mean ET values in response to variation in each parameter at well X2.	50
5.2	Range and mean of hydraulic conductivity values from pumping tests at the BHRS (Fox, 2006) and mean values from well X3 and X4 through the inversion of drawdown records using the analytical model of Malama & Johnson (2010)	56

LIST OF FIGURES

1.1	Aerial photograph of the Boise Hydrogeophysical Research Site with monitoring installations	4
1.2	Daily average Boise River discharge from Lucky Peak Dam discharge and New York Canal diversions (all in cubic feet per second) from May 1-October 1 2009.	6
2.1	Change in depth to water table with time in well X2 at the BHRS. δS is the net change in water table position for 1 period (1 day) and R [L/T] is the net recovery rate of the groundwater.	12
2.2	Instantaneous and cumulative ET flux at the water table for a daily cycle modeled after Batra <i>et al.</i> (2006). ET [in mm] is plotted against time in hours after sunrise (t_0) for a time period of $t_{day} = 15$ hours	14
2.3	Conceptual model of the semi-infinite flow domain of the Malama & Johnson (2010) model. ET flux is applied as a forcing function at the water table uniformly over an area x distance from the river (with a known head elevation). Drawdown is calculated over the aquifer thickness (b) at point x	15

2.4	Simulated drawdown record (B) at a well 60 m from river boundary in response to an ET signal (A) with amplitude (Q) of 16 mm/day and a length of 12 hours ($t_{day} = 0.5$). Note the incomplete recovery of the water table due to water lost to ET	17
2.5	Soil moisture data collected near well X2 at the BHRS in 2010 showing the decrease in soil moisture over the summer after a wet spring. Lowest values (Z position AMSL) for each time profile are recorded less than 15 cm above the water table.	18
3.1	Outline of data used in calculation of ET and aquifer drawdown response. .	19
3.2	Comparison of modeled net radiation calculated from solar radiation at AgriMet site versus observed net radiation at the BHRS as measured with portable meteorological station (June 30, 2010).	21
3.3	Comparison of soil heat flux model (Moran <i>et al.</i> , 1989) results against analytical calculation of soil heat flux at the BHRS (June 2010).	23
3.4	Computed NDVI values at the BHRS for 2009 (A) for four wells along with (B) aggregated values for areas with higher observed vegetation density (X2, X3, X4) compared to a lower vegetation density control well (C1). . .	26
3.5	Plot of NDVI versus time showing NDVI values derived from Landsat (averaged over four 30×30 m pixels) and from MODIS (500 m pixel) over the BHRS and surrounding area.	28

4.1	Aerial photograph (2009 NAIP, 1 m resolution) provides the base image of the BHRS. The grid overlain on the photo represents NDVI values from July 5, 2009 Landsat 5 data. Each grid cell represents a 30x30m pixel (spatial resolution of the satellite data) and is plotted here in grayscale with lighter squares representing higher NDVI values (more dense vegetation) and darker squares representing lower NDVI.	33
4.2	ET amplitude from mid-May through October in 2009 at the BHRS for four wells. The X labeled wells are located in more densely vegetated areas (see Figure 4.1) and well C1 is located in the central well field that is noticeably more void of vegetation. Calculated ET amplitudes reflect this difference in vegetation cover.	34
4.3	ET amplitude [mm/day] from May 18 - November 1 at well X2 plotted against daily $R_{n,max}$; these $R_{n,max}$ values were used to calculate daily ET flux. 36	
4.4	ET amplitude [mm/day] from May 18 - November 1 at well X2 plotted against daily average air temperature [$^{\circ}C$] at the BHRS that were used to calculate daily ET flux.	37
4.5	ET amplitude [mm/day] from May 18 - November 1 at well X2 plotted against calculated NDVI [-] from Landsat data at the BHRS that were used to calculate daily ET flux. Points on the NDVI line indicate values retrieved from Landsat images while the lines connecting points are linear interpolations for days with no satellite overpass.	38

4.6	Well hydrograph from July 3-July 6, 2009 showing diurnal fluctuations of the water table in response to evapotranspiration at the BHRS at well X2. Periods of drawdown are shaded yellow with the associated length of time displayed on the graph	39
4.7	ET amplitude (A) versus well drawdown (B) over the year for four wells at the BHRS. Although X4 has the highest calculated ET rates, daily drawdown is consistently lower than the other wells due to its proximity to the river.	40
4.8	Results of ET calculated at well X2 over 5 days using the radiation based method from Batra <i>et al.</i> (2006) compared to ET calculated from well hydrographs (White, 1932)	42
4.9	Results of ET calculated at well X4 over 5 days using the radiation based method from Batra <i>et al.</i> (2006) compared to ET calculated from well hydrographs (White, 1932)	43
4.10	Modeled water table elevation at the well with increasing distance from the river edge. Aquifer conductivity and ET flux are held constant and the distance between the well and river edge [x] is changed for each model run.	44
4.11	Modeled water table elevation at the well with increasing ET amplitude [Q]. Aquifer conductivity and the distance from the river edge are held constant and the ET flux is changed for each model run.	45
4.12	Modeled water table elevation versus observed (A) at well X3 and (B) at well X4 in July, 2009. Modeled results here use average aquifer hydraulic conductivity values defined in Table 1.1, and river edge distances (x) of 53m and 36m, respectively.	46

5.1	ET amplitude at X2 from May 18-August 1, 2009 plotted with results of Monte Carlo simulation for parameter sensitivity analysis for (A) temperature, (B) net radiation, and (C) NDVI. Seasonal mean ET amplitude (13.44 mm/day) is shown as the red line bounded by maximum and minimum average values for seasonal ET as a result of the simulation.	49
5.2	Regression analysis for calculated ET amplitude versus net radiation, NDVI, and average air temperature for dates May 18-September 1 2009	51
5.3	(A) Instantaneous ET flux [mm/day] during a 24 hour period ($t = 1$). For this example t_{day} , time over which $f(t)$ is applied, is equal to 0.625 (15 hours). The amplitude of the curve is equal to the reported Q values for ET. (B) Cumulative ET flux [mm] over a 24 hour period.	53
5.4	Using calculated ET and water records from in-well transducers, along with aquifer system parameters such as distance from river and saturated aquifer thickness, hydraulic conductivity is estimated using a least squares optimization.	55

Chapter 1

INTRODUCTION

Evapotranspiration (ET) has been estimated by many different methods using data related to vegetation, soil moisture (along with other properties of the unsaturated zone), and meteorological parameters. The majority of methods involve energy or mass balance equations that require extensive data acquired at a specific site and are typically related to soil moisture fluctuations in the unsaturated zone. However, riparian zones in semi-arid regions often exhibit high rates of evapotranspiration in spite of low soil moisture content due to vegetation that is able to withdraw water from shallow aquifers. Well hydrographs in these regions often display diurnal fluctuations of the water table due to vegetation drawing from the shallow aquifer to meet transpiration demands.

This thesis aims to better define the relationship between ET, the saturated zone, and a river boundary in riparian areas using the observed and modeled drawdown at fully penetrating wells in an unconfined aquifer in response to daily ET flux. In a system dominated by ET where diurnal fluctuations of the water table are observed, using ET as a boundary condition at the water table will allow drawdown to be modeled if the aquifer is well characterized. Conversely, if ET is well characterized, aquifer parameters like hydraulic

conductivity and specific storage can be estimated if the boundary conditions are known. Addressing spatial variations in ET magnitude and accounting for spatial differences regarding the distance to the river (x) at different wells will further test the analytical draw-down model and sensitivity to daily changes in ET.

1.1 Previous Work

Batra *et al.* (2006) present a method for computing ET that relies primarily on remotely sensed parameters and uses a modified version of the Priestley-Taylor equation (Priestley & Taylor, 1972). Gribovszki *et al.* (2008) used similar parameters but compared these to observed diurnal fluctuations in the groundwater elevation to estimate ET. In regions dominated by phreatophytic vegetation, these diurnal fluctuations of the water table can be seen as a direct response to an increase in plant transpiration and are therefore positively correlated with ET (Loheide II *et al.*, 2005; Butler Jr. *et al.*, 2007).

White (1932) presented some of the first work relating ET magnitude to well hydrographs. His approach calculates the groundwater component of evapotranspiration (ET_g) from the empirical relationship $ET_g = S_y \delta S + R$ where S_y [dim] is the specific yield, δS [L/T, presented as T=1 day] is the net change in water table position for 1 period (1 day), and R [L/T] is the net recovery rate of the groundwater. R can be calculated over a time of day (commonly 00:00 - 04:00 AM) where ET is assumed to be negligible with R equal to change in head [L] over change in time [T] or $\partial h / \partial t$.

Loheide II *et al.* (2005) found that the method of White (1932) tends to overestimate ET and they set forth new guidelines for its use including a more thorough method for estimating the readily available specific yield (S_y^*) for sub-daily testing. More recently, Gribovszki *et al.* (2008) applied the Dupuit approximation for saturated flow to more accurately relate the recovery rate (R) to water level fluctuations and show that for riparian phreatophytes, hydraulic head changes in response to transpiration occur across the entire saturated zone. Through numerical simulation accounting for unsaturated and saturated flow, Shah *et al.* (2007) found that almost all ET comes from groundwater when the water table is within a meter of land surface. The extinction depth for which groundwater is the source of ET is positively related to the amount and type of vegetation cover (Shah *et al.*, 2007), which further supports the idea that the vadose zone plays a limited role in ET in this type of system.

This thesis builds upon the work cited above and applies an analytical solution that relates groundwater flow to ET (Malama & Johnson, 2010), and uses this solution to model ET-induced drawdown at the Boise Hydrogeophysical Research Site (BHRS). These results will be compared to the observed well records to validate the model, estimate aquifer parameters with known ET forcing, and further the understanding of the relationship between the river boundary and shallow aquifer system.

1.2 Site Overview

The Boise Hydrogeophysical Research Site (BHRS) is a research well field and hydrologic processes observatory located 12 km southeast of downtown Boise, ID adjacent to the Boise River (Figure 1.1). The unconfined aquifer consists of unconsolidated cobble, gravel,

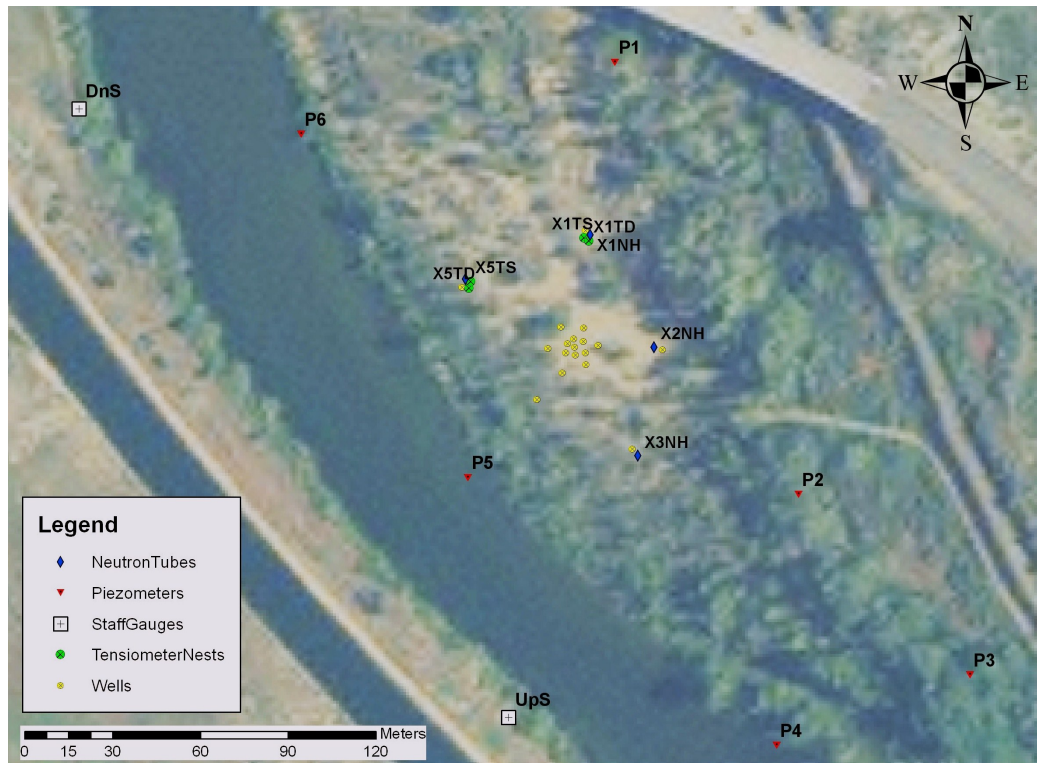


Figure 1.1: Aerial photograph of the Boise Hydrogeophysical Research Site with monitoring installations

and sand fluvial deposits approximately 18 m thick and is underlain by a continuous clay layer (Barrash *et al.*, 2006; Barrash & Clemo, 2002). The 18 wells emplaced at the site are fully screened and fully penetrate the aquifer. Aquifer parameters have been estimated by hydrological (pumping and slug tests) and geophysical techniques and mean values based on fully penetrating pumping tests are presented in Table 1.1 (Fox, 2006).

The Boise River flows year round with discharge controlled by discharges from Lucky Peak Dam and discharges and diversions from Diversion Dam (operated by US Department of the Interior, Bureau of Reclamation), the latter of which is located about 600 meters upstream from the site. Spring runoffs are generally high, fed from snowmelt in

Parameter	Mean	Maximum	Minimum	Units
K_r	7.59×10^{-4}	1.29×10^{-3}	5.13×10^{-4}	m/s
K_z	6.61×10^{-4}	1.29×10^{-3}	3.80×10^{-5}	m/s
S_s	4.07×10^{-5}	1.29×10^{-4}	3.31×10^{-5}	m^{-1}
S_y^*	0.036	0.070	0.013	[dim]

Table 1.1: Mean aquifer parameters resulting from analytical modeling of pumping tests (73 pumping well-observation well pairs) at the BHRS (Fox, 2006).

* S_y values are recognized to be lower than may be expected for unconsolidated coarse fluvial aquifers although similar values have been obtained from aquifers tests of relatively short duration (Barrash *et al.*, 2006) and have generally been observed in analytical solutions (Neuman, 1972).

the upper reaches of the Boise River drainage. Discharge in the lower Boise River (adjacent to the BHRS) can be relatively high and variable due to periodic releases from the dams. The summer months exhibit generally steady flow while water is fed to irrigation canals, and river flow decreases in the fall and winter months when the irrigation canals are no longer in use and flows are restricted to increase storage behind the dams. All data concerning discharge in the Boise River are made available by the Bureau of Reclamation (<http://www.usbr.gov/pn/hydromet/boipaytea.cfm>) and daily averages of discharge and diversions for May-October, 2009 are seen in Figure 1.2.

Vegetation in the riparian zone at the BHRS is dominated by cottonwoods (*Populus* spp.) and coyote willow (*Salix exigua*), which are both known phreatophytes. Previous work at the BHRS has noted root growth into the wells, which can be thick in the uppermost portion of some wells, and diurnal fluctuations of the water table (Barrash *et al.*, 2002; Cardiff *et al.*, 2009). Phreatophytic vegetation obtain a significant amount of water from shallow aquifers and the capillary fringe and are common in riparian zones, particularly in semi-arid regions. Accessibility to the saturated zone allows these plants to thrive in areas

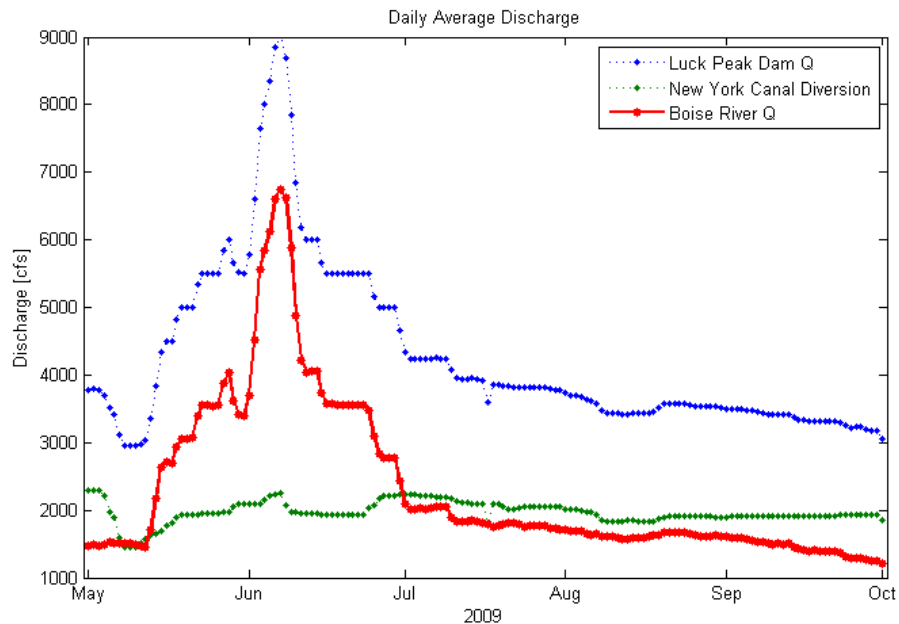


Figure 1.2: Daily average Boise River discharge from Lucky Peak Dam discharge and New York Canal diversions (all in cubic feet per second) from May 1-October 1 2009.

where unsaturated soil moisture is near residual amounts through much of the year.

1.3 Objectives

The first objective of this thesis is to accurately quantify and characterize the evapotranspiration signal at the BHRS following the method of Batra *et al.* (2006). To increase temporal resolution in the data, a hybrid approach will be used to integrate daily weather data into the ET equation. Completion of this objective will produce a dataset of daily ET flux at the site that varies spatially with vegetation cover. The second objective of this thesis is to use the calculated ET fluxes to analytically solve for daily drawdown in the wells using the method of Malama & Johnson (2010). These results will be compared against observed drawdown to validate the analytical model and the parameters used within. For

comparison, water table levels in wells with different surrounding vegetation densities and distances from the river edge will be monitored for a full growing season to observe how daily ET rates change during the year across the BHRS.

As noted before, diurnal fluctuations of the water table have been observed at the BHRS but, prior to this work, were not collected over the full growing season. Well record data from 2009 consist of daily records of water table levels in multiple wells throughout the spring-summer-fall growing season, when vegetation cover is changing and ET magnitude is expected to be greatest. The final objective will be to use the observed head records and calculated ET values to estimate hydraulic conductivity at the BHRS. These results will then be compared to the observed drawdown in the wells and will be used to further test the analytical model and investigate relative water contribution from the river and aquifer as a function of well distance from the river edge.

Chapter 2

THEORY AND MODEL DEVELOPMENT

Evapotranspiration (ET) is the sum of the water transferred into the atmosphere through evaporation and transpiration. Evaporation can occur from standing water on the ground surface and leaves of plants or from shallow soils. Evaporation is a function of solar energy but, in general, is driven by a vapor pressure gradient with the atmosphere. Transpiration encompasses any water that is evaporated from within leaves of plants and diffused into the atmosphere from the plant stomata (Dingman, 2002). The terminology “shallow, near-surface” is used here to stress the fact that plants can tap into water from multiple water sources below the ground surface where the atmospheric vapor pressure gradient is not a factor. Batra *et al.* (2006) cites the three major factors controlling ET as: (1) the availability of water, (2) the amount of available radiant energy, and (3) an atmospheric transport mechanism to remove the water vapor away from the surface.

At larger spatial scales, a mass balance approach is often used to quantify water in the system. This takes the form

$$\frac{\partial S}{\partial t} = \text{Input} - \text{Output} \quad (2.1)$$

where the difference between input and output is the change in storage. It is often assumed that change in storage is negligible over the course of a year and input should equal output in the system. From the watershed perspective, the water balance equation can be shown as

$$P + GW_{in} = Q + ET + GW_{out} \quad (2.2)$$

where inputs include precipitation (P) and groundwater flow into the watershed (GW_{in}), while outputs include (ET) and groundwater (GW_{out}) and streamflow (Q) leaving the watershed (Dingman, 2002).

Using the mass balance approach presented above, ET in a hydrologic system can be calculated from the residuals of the inputs and outputs of the system if change in storage is assumed to be negligible ($\frac{\partial S}{\partial t} = 0$) following

$$ET = P - Q \quad (2.3)$$

Estimating ET from residuals (or unaccounted for water) is not preferred as it includes error in measurement from all other variables and is only valid at large spatial scales (i.e., watersheds). Precipitation measurements are usually averaged over large areas and there are difficulties measuring spatial variability. Water lost to groundwater flow is difficult to quantify. However, ET remains difficult to estimate directly and is often estimated in this fashion.

In this thesis, the discussion will be limited to ET in the riparian zone in a temperate semi-arid environment. This area is an important ecosystem that can support a variety of

plants and animals in often very dry regions. Estimates of ET are difficult in these areas based on the unique geometry of the riparian zone. Many are long, narrow, and sinuous as they follow the contours of a river (Goodrich *et al.*, 2000). This geometry violates the requirements for some micro-meteorological flux measurements such as eddy covariance (Hippis *et al.*, 1998). The focus here will be on using a method that employs remotely sensed parameters as well as site measurements to estimate ET.

2.1 Transpiration

Plant transpiration is a function of many different variables but the movement of water can still be represented as a mass balance problem. It is important to consider the potential evapotranspiration (PET) in relation to the actual evapotranspiration. Key to PET is that vegetation has an unlimited amount of water and heat storage effects are negligible (Dingman, 2002). A major difficulty in calculating transpiration flux is moving from the leaf scale to the canopy scale to an entirely larger, regional scale. This problem is amplified in areas of mixed vegetation as each species can have unique transpiration characteristics.

For this reason, in this thesis, vegetation is accounted for indirectly by using a normalized difference vegetation index (NDVI) value obtained from remotely sensed satellite data. Landsat 5 data are used to obtain a unique NDVI for each 30x30m pixel in the study area. This thesis is limited to the temperate, semi-arid riparian zone with focus on a special group of plants (phreatophytes) that have an effectively unlimited source of water, even in semi-arid conditions.

2.2 Phreatophytes and Diurnal Fluctuations of the Water Table

Phreatophytes are plants that obtain a substantial amount of water from the saturated zone and/or the capillary fringe. Common phreatophytes include cottonwood (*Populus* spp.), greasewood (*Sarcobatus vermiculatus*), salt cedar (*Tamarix chinensis*), willows (*Salix*), and Arizona mesquite (*Prosopis velutina*) (Beschta, 2005). These types of vegetation are common in the riparian zone where the water table is often shallow, and in semi-arid or arid regions where water is limited. Since these plants are in direct contact with the saturated zone, daily changes in water table levels can be seen as a direct response to vegetation transpiration (assuming other secular influences are negligible or otherwise accounted for). Transpiration generally follows the diurnal solar radiation cycle causing the water table to decline throughout the day as the plants move the water from the saturated zone out through the leaves. During the night, transpiration becomes negligible and the water table recovers due to net inflow (Loheide II *et al.*, 2005).

Figure 2.1 shows the depth to water below land surface on a daily cycle at the BHRS where plants are drawing water from the saturated zone during the day with recovery at night. Recovery rate and change in storage (R and δS , respectively) calculated using the method of White (1932) are labeled in the figure. The recovery rate calculated here, and generally using the method of White (1932), is a linear approximation of recovery rate starting when ET is assumed to be negligible. Loheide II *et al.* (2005) found this assumption to be reasonable when a value of readily available specific yield could be determined. Readily available specific yield (often noted as S_y^*) is lower than traditionally defined specific yield

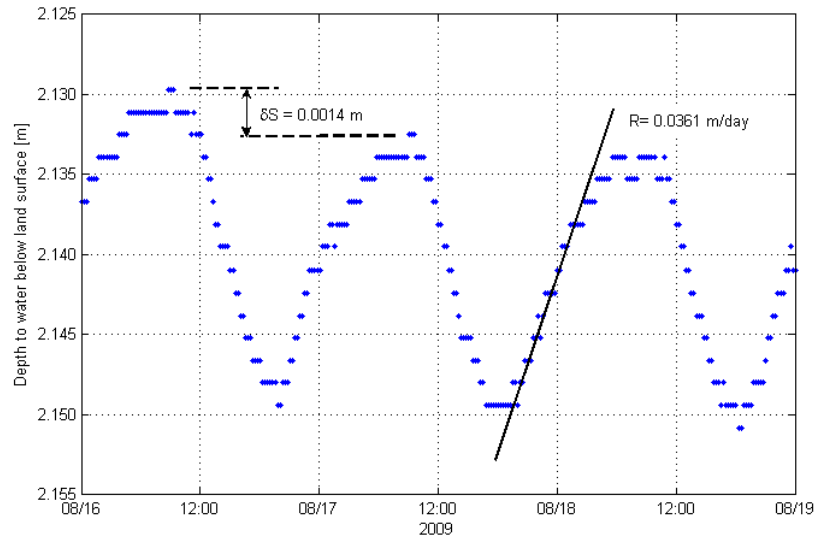


Figure 2.1: Change in depth to water table with time in well X2 at the BHRS. δS is the net change in water table position for 1 period (1 day) and R [L/T] is the net recovery rate of the groundwater.

and is used to describe water used during a short period of time, typically less than 12 hours (Meyboom, 1967; Loheide II *et al.*, 2005). Troxel (1936) first noted that the recovery rate is non-linear and the curvature seen nearing peak recovery in well hydrographs shows that the rate is not constant in time. Time-dependent recovery rate is formulated by Loheide II (2008), but the original method of White (1932) is limited by the assumption of constant recovery rate.

2.3 Evapotranspiration

With the many factors that need to be considered when estimating evapotranspiration, collection of data via remote sensing techniques, particularly orbiting satellite, is often preferred because it reduces the amount of ground data that need to be collected. Evapo-

transpiration can be estimated using a derivation of the Priestley-Taylor equation (Jiang & Islam, 2001)

$$\lambda ET = \phi \left(\frac{\Delta}{\Delta + \gamma} \right) (R_n - G) \quad (2.4)$$

which has the advantage of containing variables that can be derived from remote sensing data along with common meteorological data. These parameters include soil heat flux (G [W/m^2]), net radiation (R_n [W/m^2]), and a dimensionless, empirical parameter (ϕ) that is the actual evaporation rate over the equilibrium evaporation rate (here, $\phi=1.26$ for the BHRS setting, see Section 3.1 and Equation 3.5). The slope of the saturated vapor pressure curve (Δ) and the psychrometric constant (γ [kPa/K]) are functions of air temperature. ET is the evapotranspiration mass flux ($kg/m^2 \cdot s$) and λ is the latent heat of vaporization of water (J/kg). Combining the relation between G and R_n presented by Batra *et al.* (2006)

$$G = 0.583 \exp(-2.13NDVI)R_n, \quad (2.5)$$

where R_n is modeled after Bisht *et al.* (2005) as

$$R_n(t) = R_{n,max} \sin(\omega t), \quad (2.6)$$

and the Priestley-Taylor Equation (2.4), daily ET amplitude can be quantified by

$$Q = \frac{R_{n,max} \phi \Delta}{\rho \lambda (\Delta + \gamma)} [1 - 0.583 \exp(-2.13NDVI)] \quad (2.7)$$

where Q is the amplitude of ET flux (m/s) at the water table due to evapotranspiration and $R_{n,max}$ is the maximum net radiation measured during the day (Batra *et al.*, 2006; Bisht

et al., 2005). The daily ET function then becomes a smooth sine curve described by

$$f(t) = \frac{ET}{\rho} = \begin{cases} Q \sin(\omega t) & \forall t \in [0, t_{day}] \\ 0 & \forall t > t_{day}. \end{cases} \quad (2.8)$$

where ρ is the density of water and $\omega = \pi/t_{day}$, where $t_{day} = t_{set} - t_{rise}$ with t_{set} and t_{rise} the times, where net radiation becomes negative and positive, respectively. Figure 2.2 shows this function over a 24 hour period where the t_{day} is the time from sunrise to sunset (15 hours, here) and $Q = 14$ mm/day.

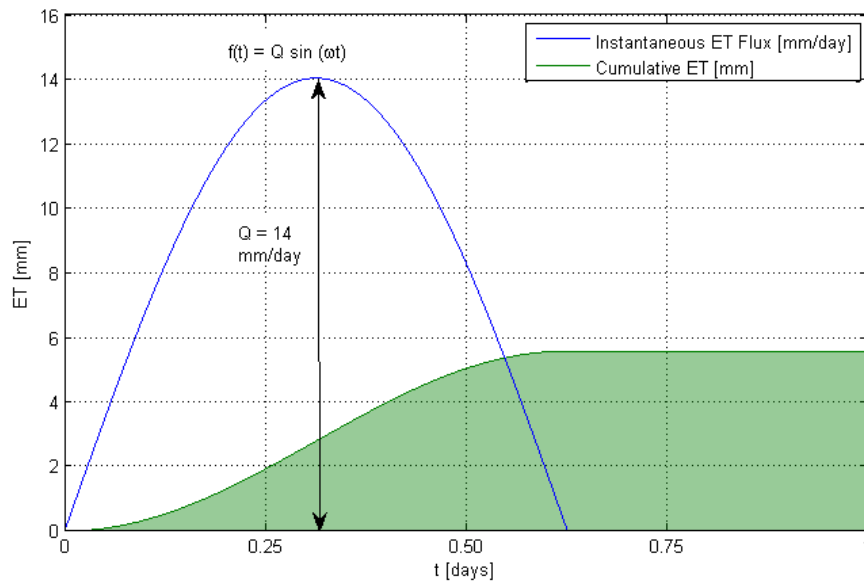


Figure 2.2: Instantaneous and cumulative ET flux at the water table for a daily cycle modeled after Batra *et al.* (2006). ET [in mm] is plotted against time in hours after sunrise (t_0) for a time period of $t_{day} = 15$ hours

2.4 Analytical Drawdown Model

The analytical model developed in Malama & Johnson (2010) is a solution to hydraulic head changes in an unconfined aquifer in response to evapotranspiration at the water table. The water table is treated as a moving material boundary following the work of Neuman (1972) and flow in the unsaturated zone is ignored as drawdown in response to ET is typically small. The focus of this thesis will be on the semi-infinite flow domain (Figure 2.3) with head in the Boise River serving as the lateral boundary condition. Two dimensional

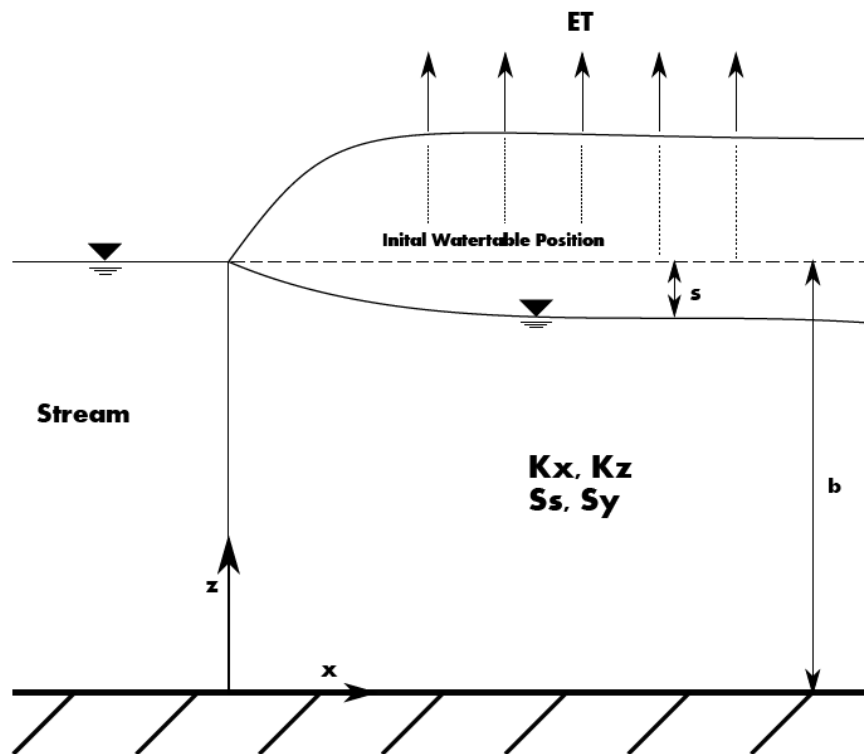


Figure 2.3: Conceptual model of the semi-infinite flow domain of the Malama & Johnson (2010) model. ET flux is applied as a forcing function at the water table uniformly over an area x distance from the river (with a known head elevation). Drawdown is calculated over the aquifer thickness (b) at point x .

flow is considered with a finite vertical extent ($z = b$) and semi-infinite lateral extent ($x = 0$)

at river-land interface). The ET flux is applied uniformly at the water table at the x position for each well. Drawdown (s) from the initial steady state follows

$$\frac{1}{\alpha_z} \frac{\partial s}{\partial t} = \frac{K_x}{K_z} \frac{\partial^2 s}{\partial x^2} + \frac{\partial^2 s}{\partial z^2} \quad (2.9)$$

where $\alpha_z = \frac{K_z}{S_s}$ (vertical hydraulic diffusivity) and is solved with the aforementioned initial condition

$$s(x, z, t = 0) = 0 \quad (2.10)$$

and boundary conditions with no leakage at the bottom boundary ($z = 0$)

$$\left. \frac{\partial s}{\partial z} \right|_{z=0} = 0. \quad (2.11)$$

and the ET function at the water table ($z = 1$)

$$\left. \frac{\partial s}{\partial z} \right|_{z=1} = \frac{1}{\sigma} \left. \frac{\partial s}{\partial z} \right|_{z=1} - f(t) \quad (2.12)$$

where $\sigma = bS_s/Sy$ and $f(t)$ as presented in Equation 2.8.

The ET function is applied at the water table with the modeled head presented in the analytical solution being a depth-averaged drawdown over the saturated thickness of the well. Figure 2.4 shows the simulated, depth-averaged response in the well to the ET forcing for a single day. Here, $t = 0$ corresponds to the time when net radiation becomes positive. Note that peak drawdown occurs after the peak ET flux as long as the ET rate is greater than the aquifer recharge rate.

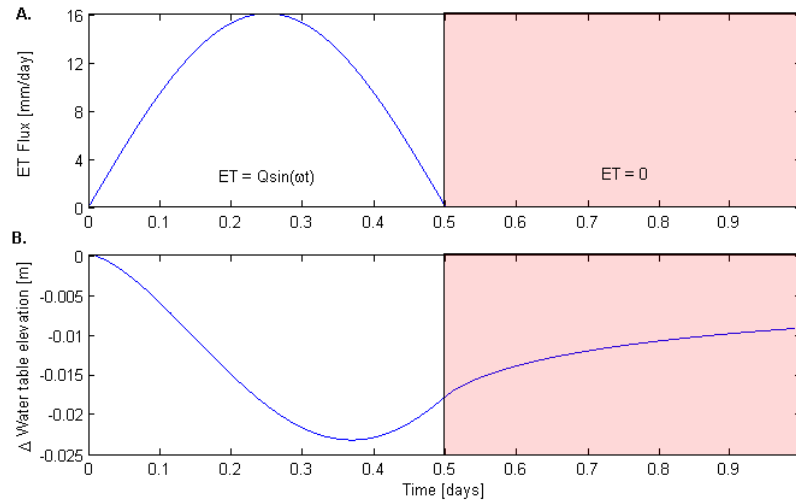


Figure 2.4: Simulated drawdown record (B) at a well 60 m from river boundary in response to an ET signal (A) with amplitude (Q) of 16 mm/day and a length of 12 hours ($t_{day} = 0.5$). Note the incomplete recovery of the water table due to water lost to ET

Following the work of Shah *et al.* (2007), water contribution from the unsaturated zone is neglected and all available water for ET is assumed to be from the saturated zone. This is also supported by White (1932) who found that in riparian zones dominated by phreatophytes, groundwater is the dominant source of water lost to the atmosphere. Further support of this assumption is seen locally at the BHRS through recent records of soil moisture (Figure 2.5) and tension head that show a continued drying of the unsaturated zone over the summer and into fall.

This thesis presents the addition of actual daily evapotranspiration estimates based on spatial vegetation heterogeneity over the BHRS. Previous work used an average ET magnitude to model expected drawdown. The present work addresses daily variations in ET magnitude as well as spatial differences regarding the distance to the river (x) at different wells to further test the analytical model and sensitivity to daily changes in ET.

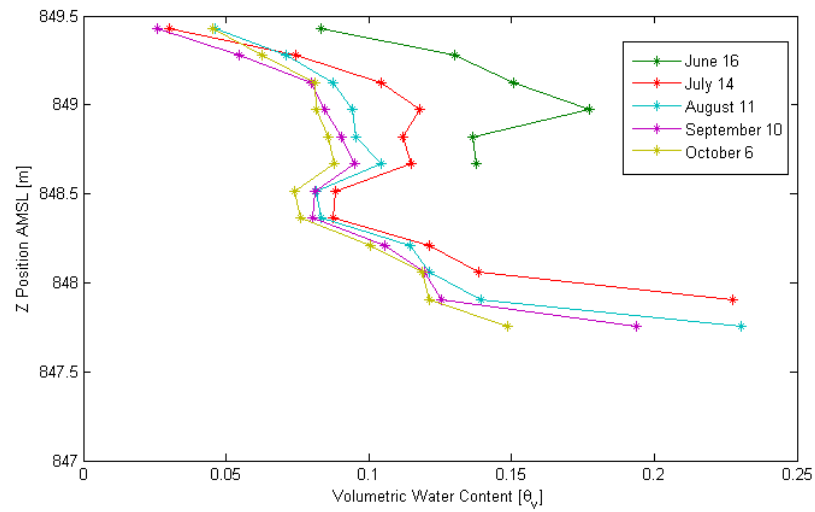


Figure 2.5: Soil moisture data collected near well X2 at the BHRS in 2010 showing the decrease in soil moisture over the summer after a wet spring. Lowest values (Z position AMSL) for each time profile are recorded less than 15 cm above the water table.

Chapter 3

METHODS

In this chapter, the methods used to quantify ET (in addition to a description of the parameters needed to calculate ET) and aquifer and river parameters are outlined. A flow chart is presented in Figure 3.1 to better visualize how the measurements and calculations relate. Recent tests are described that validate initial assumptions relating to ET parameters that were only available off site. Instrumentation and collection methods are also described

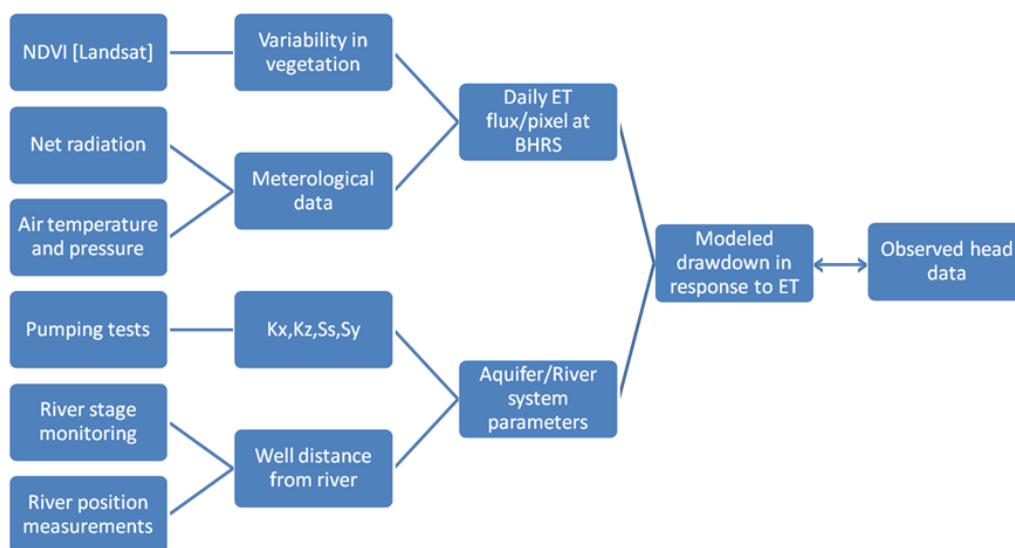


Figure 3.1: Outline of data used in calculation of ET and aquifer drawdown response.

at the BHRS for the data collection period used in the analyses in this thesis.

3.1 Characterization of Daily ET

A single diurnal cycle of the evapotranspiration cycle from Batra *et al.* (2006) has the form

$$f(t) = \frac{ET}{\rho} = \begin{cases} Q \sin(\omega t) & \forall t \in [0, t_{day}] \\ 0 & \forall t > t_{day} \end{cases} \quad (3.1)$$

where ρ is the density of water and Q (Equation 2.7) is the amplitude of the ET mass flux. To solve Equation 2.7 for any given day the following site-specific parameters are needed: $R_{n,max}$, NDVI and air temperature. The air temperature at the BHRS was recorded using a Solinst Barologger. In addition to recording air temperature (at 10 ft above land surface in the canopy of a black cottonwood tree, which is non-standard, but data agree well with temperature data recorded near-site), atmospheric pressure was recorded to correct for total pressure transducers used at the site to measure water levels in the wells. Net radiation measurements $R_{n,max}$ were not available at the BHRS but were measured at a full AgriMet weather station located 9 kilometers northwest (315° azimuth, relative to the center of the well field at the BHRS).

The AgriMet station records hourly solar radiation and, following the guidelines set forth by the Food and Agriculture Organization (Allen *et al.*, 1998), net radiation was estimated (supporting calculations are given in Appendix B). Bisht *et al.* (2005) present a sinusoidal model for net radiation that requires only a single measurement from the satellite each day. The model is used but radiation data are obtained from the local weather station instead of satellite retrieval to improve temporal resolution. To test the validity of using

AgriMet data for modeling radiation measurements at the BHRS, a portable weather station capable of measuring net radiation was deployed at the BHRS. Values from the portable weather station on-site compared favorably with those estimated from the AgriMet station following FAO procedure over the same time period (Figure 3.2).

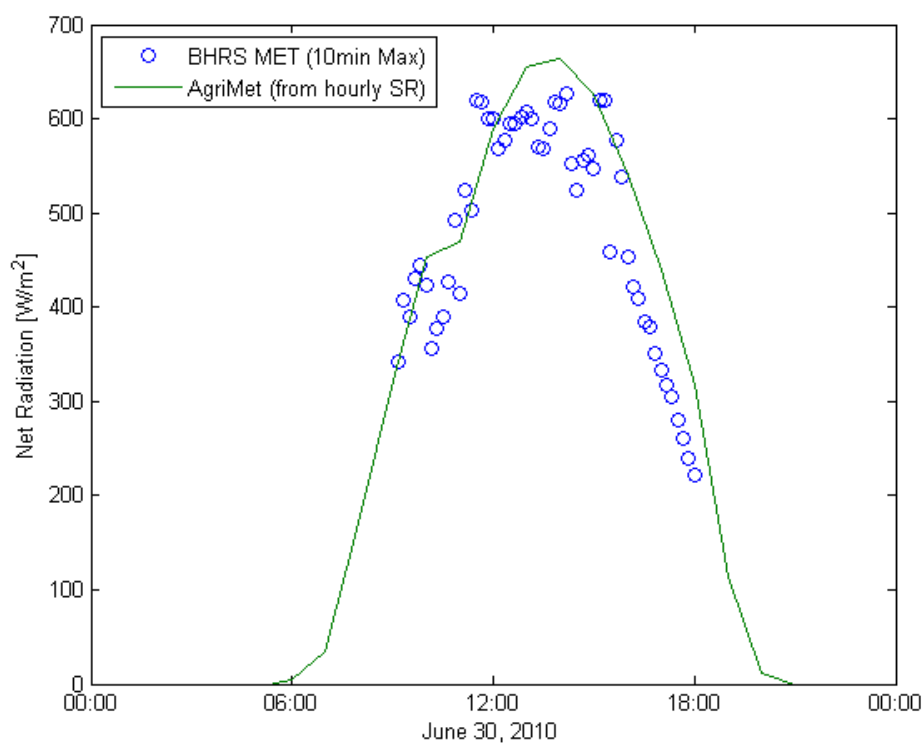


Figure 3.2: Comparison of modeled net radiation calculated from solar radiation at AgriMet site versus observed net radiation at the BHRS as measured with portable meteorological station (June 30, 2010).

The method of parameterizing soil heat flux in terms of net radiation and NDVI (Batra *et al.*, 2006; Moran *et al.*, 1989) was also tested to validate the use of the model at the BHRS. Current instrumentation does not provide direct measurements of soil heat flux (G),

which needs to be accounted for in the energy balance. Moran *et al.* (1989) show that

$$G/R_n = 0.583 \exp^{-2.13NDVI} \quad (3.2)$$

so that soil heat flux increases (proportionally with net radiation) as vegetation cover decreases. Although the method has been used previously with success and is well documented in the literature (Moran *et al.*, 1989; Bisht *et al.*, 2005; Batra *et al.*, 2006), calculations were made at the BHRS to ensure the energy equations were in balance. Soil heat flux was calculated for a three-day period in June of 2010 using an analytical model with estimated soil heat conductivity based on dry grain size distribution seen at the site and soil temperature gradients calculated at the near surface from tensiometer nests installed at the site. Analytical and modeled results following Batra *et al.* (2006) are graphed with net radiation measurements in Figure 3.3. Modeled soil heat flux results agree in timing and magnitude with those from analytical calculations. In maintaining consistency within this paper, net radiation goes to zero at times $t \geq t_{day}$, so modeled G goes to zero while the analytical solution shows the negative heat flux overnight.

Normalized Difference Vegetation Index (NDVI) is a value commonly determined from satellite data that quantifies the amount of green vegetation in a given pixel (i.e., area). NDVI calculations are based on the differential reflectance values of light due to the structure (internal and external) and color of the plant. Chlorophyll in the plant absorbs blue and red light (450-495 nm and 620-750 nm, respectively) for use in photosynthesis and reflects more of the green light (495-575 nm). Living vegetation will highly reflect infrared light. Whereas green light reflection is controlled by chloroplasts at the plant leaf surface interface, infrared reflection is due to the internal structure of the mesophyll. It should be noted that NDVI is a calculated ratio from a specific sensor (i.e., the thematic mapper

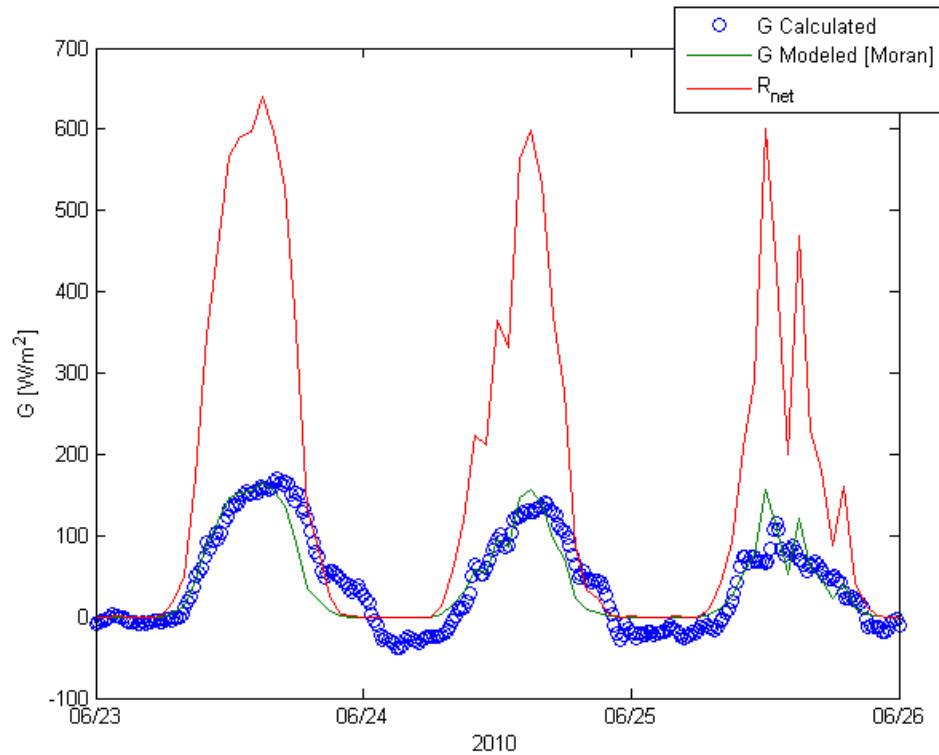


Figure 3.3: Comparison of soil heat flux model (Moran *et al.*, 1989) results against analytical calculation of soil heat flux at the BHRS (June 2010).

(TM) on Landsat 5). Normalizing this difference in reflectance values provides the NDVI calculation (Liang, 2004):

$$NDVI = \frac{Infrared - Red}{Infrared + Red} \quad (3.3)$$

It is recommended that NDVI values should be reduced to radiances when comparing values over time or from two different sensors (Price, 1987). For continuity, all NDVI presented here are derived from radiances.

Clear sky (less than 10 % cloud cover) Landsat 5 TM satellite images were used to

calculate NDVI at the BHRS. Landsat 5 TM was chosen because the smaller footprint (30m pixel) is better suited to the narrow riparian corridor than MODIS (500m pixel). Landsat data have the added benefit of being freely distributed for download through the USGS. Normal temporal resolution for Landsat data is 16 days but the BHRS benefits from satellite path overlap (path 41 and 42, row 30), which can provide 8 day resolution. Cloud cover can limit the number of images available to calculate NDVI, but Table 3.1 lists the images that fit the criteria for NDVI calculations. NDVI for each image was calculated with ENVI software using the built-in NDVI tool following Equation 3.3. For Landsat 5 TM, the red and near infrared bands are bands 3 (0.63-0.69 μm) and 4 (0.76-0.90 μm), respectively. The radiance value band math used by the NDVI tool in the ENVI software (ENVI, 2006) follows

$$NDVI = \frac{\text{Band 4} - \text{Band 3}}{\text{Band 4} + \text{Band 3}} \quad (3.4)$$

Preprocessing of the images included geometric corrections and radiometric corrections for dark object subtraction (Tso & Mather, 2009) and a conversion from reflectance values to radiances (Liang, 2004).

		NDVI	NDVI	NDVI	NDVI
Date	Path/Row	C1	X2	X3	X4
5/18/2009	41/30	0.2273	0.3016	0.3153	0.3396
6/3/2009	41/30	0.2131	0.3103	0.3529	0.3750
6/19/2009	41/30	0.1973	0.3488	0.4414	0.3628
7/5/2009	41/30	0.1831	0.2576	0.3153	0.3962
7/21/2009	41/30	0.2239	0.3659	0.4074	0.3739
7/28/2009	42/30	0.1969	0.2283	0.3143	0.3592
8/22/2009	41/30	0.1966	0.2661	0.3263	0.3673
9/23/2009	41/30	0.1402	0.2766	0.2941	0.2791
10/9/2009	41/30	0.1333	0.2346	0.2571	0.2941
10/16/2009	42/30	0.1688	0.1948	0.2308	0.2903
10/25/2009	41/30	0.1733	0.1667	0.1864	0.2281
11/1/2009	42/30	0.1026	0.1667	0.1746	0.1930

Table 3.1: List of clear sky days with Landsat 5 TM images for the BHRS and calculated NDVI for four wells representing four different pixels.

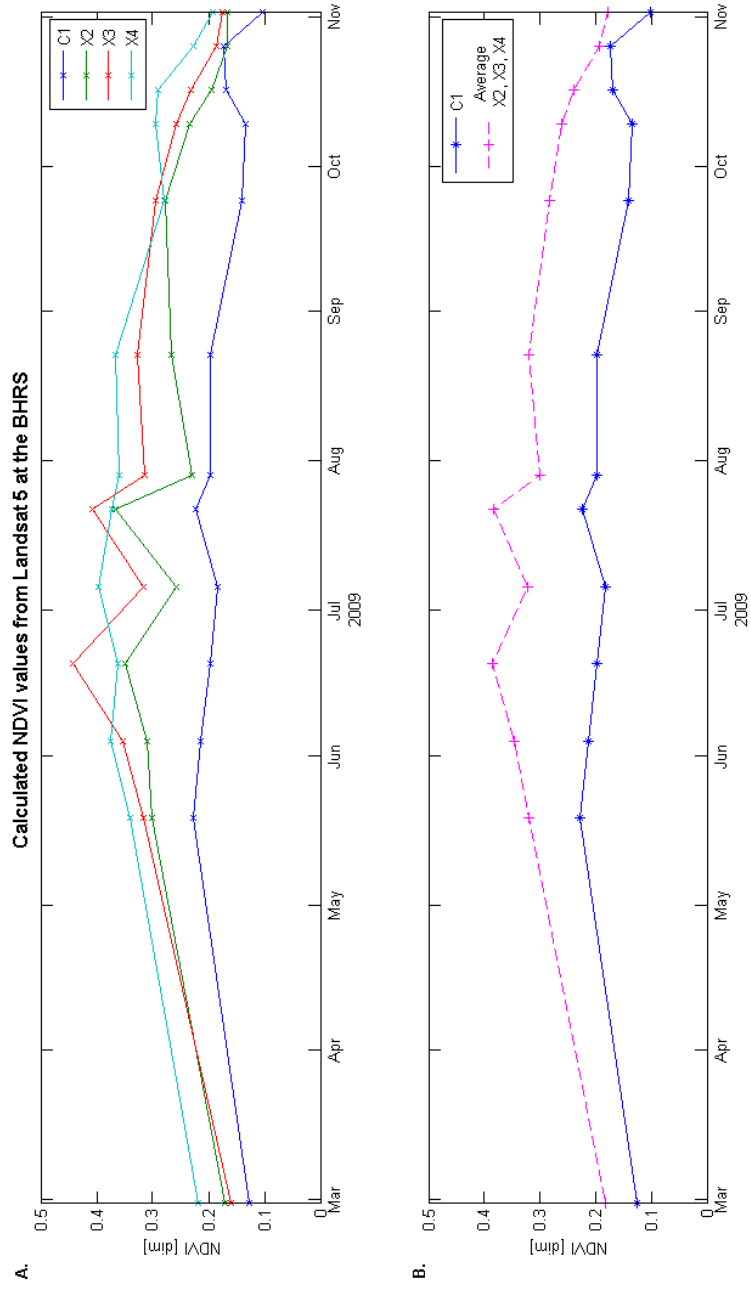


Figure 3.4: Computed NDVI values at the BHRS for 2009 (A) for four wells along with (B) aggregated values for areas with higher observed vegetation density (X2, X3, X4) compared to a lower vegetation density control well (C1).

A linear interpolation of NDVI was used between satellite images at the site. This seems justified from the small variation observed in NDVI values from May-August (Table 3.1). NDVI at the four wells, along with the interpolations between data are shown in Figure 3.4. Generally speaking, wells X2, X3, and X4 have noticeably more vegetation (than well C1) in the immediate area and the higher NDVI at these wells reflects that. Further analysis of NDVI from MODIS data (1 day temporal, 500m spatial resolution) did not provide any contrary data that might indicate regional changes in NDVI for time periods between Landsat images, but did show a slight decrease in NDVI values through August (Figure 3.5). It should be noted that absolute NDVI value is not as important as the trend in the MODIS data because the MODIS footprint (500mx500m) is significantly larger than the Landsat footprint and provides a value averaged over that larger area that is not covered by Landsat data.

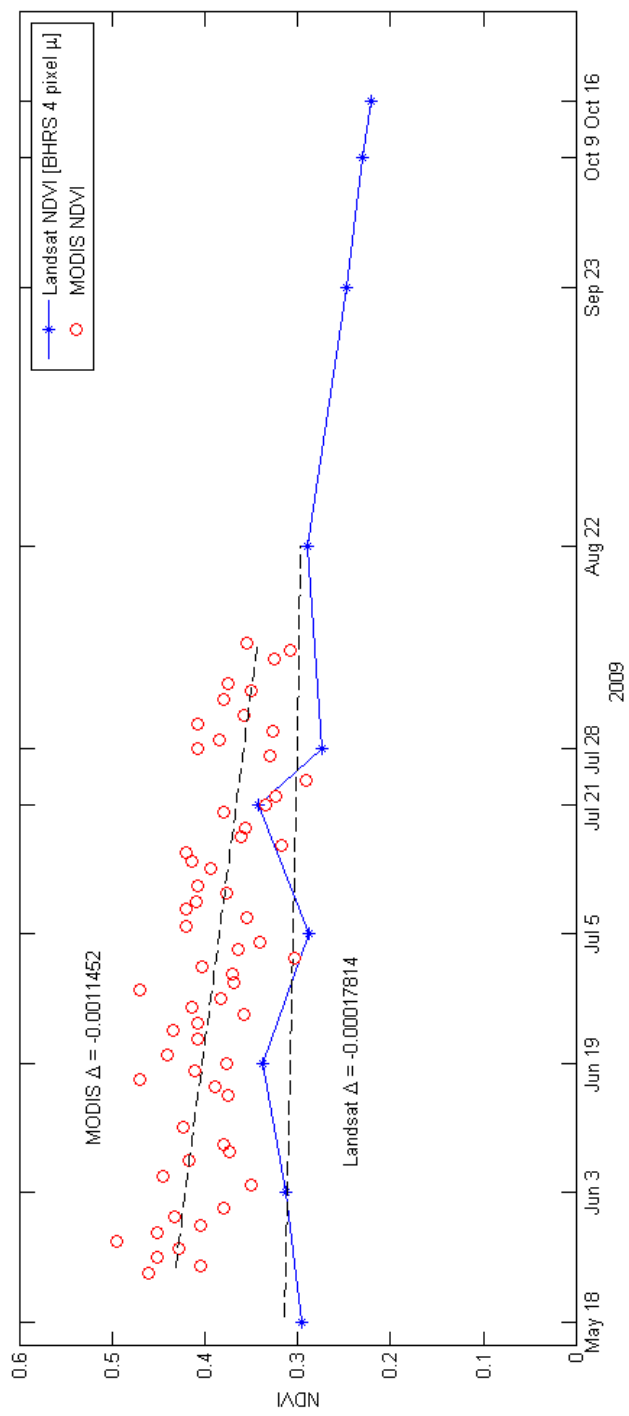


Figure 3.5: Plot of NDVI versus time showing NDVI values derived from Landsat (averaged over four 30 × 30 m pixels) and from MODIS (500 m pixel) over the BHRS and surrounding area.

The ϕ parameter in the ET equations is the only parameter that is not measured directly. ϕ is the parameter that accounts for aerodynamic and canopy resistance and is a combination of the α and β terms originally presented in Priestley & Taylor (1972). Generally speaking, this term is the actual evaporation rate over the equilibrium evaporation rate. Jiang & Islam (2001) formulate this ratio, in terms of latent energy (W/m^2), as

$$LE = \phi \left[(R_n - G) \frac{\Delta}{\Delta + \gamma} \right]. \quad (3.5)$$

From this, $\phi = 0$ represents no evaporation and $\phi = \frac{\Delta}{\Delta + \gamma}$ equals maximum evaporation. Previous work from a variety of different backgrounds, including Jiang & Islam (2001), have found this maximum $\phi = 1.26$. Eichinger *et al.* (1996) provided further support for this value through an analytical solution over a saturated surface (unlimited water).

3.2 Aquifer and River System Parameters

Forward modeling of head drawdown associated with ET requires two types of input with regard to aquifer parameters: (1) spatial data about each well including distance to river and saturated thickness and (2) hydraulic conductivity and storage parameters for the aquifer material.

River System

Spatial position of a given well with regard to the river edge position is monitored at the BHRS during the summer when the river is actively changing position due to increasing/decreasing discharge at the dam upstream of the BHRS. Late summer discharge from

Parameter	Value [units]
K_x	$6.4 \times 10^{-4} [m/s]$
K_z	$2.5 \times 10^{-4} [m/s]$
S_s	$3.8 \times 10^{-6} [m^{-1}]$
S_y	0.05

Table 3.2: Representative aquifer parameters derived from pumping tests (Barrash *et al.*, 2006; Fox, 2006) that are used for initial analytical drawdown model.

the dam is more constant resulting in a constant distance between the river and a particular well (x distance in Figure 2.3). The x distance for any day of the year is determined from a combination of hand measurements taken at the site and the development of a rating curve using the discharge from the dam to determine the position of the river edge and, therefore, the distance from the river to the well. Drawdown in the analytical model is a depth-averaged value over the saturated thickness which can be calculated based on the in-well transducers and periodic water level measurements conducted with an electric tape measure in fully penetrating wells at the BHRS to determine water table elevation.

Aquifer Parameters

To model drawdown, estimates of horizontal and vertical hydraulic conductivity (K_x and K_z), specific storage (S_s), and specific yield (S_y) are required. Pumping test analysis from Barrash *et al.* (2006) and Fox (2006) provide initial estimates for these parameters (Table 3.2).

3.3 Well Monitoring

Monitoring wells for this study were selected to represent areas with strong vegetation cover (X2, X3, X4) and little vegetation cover (C1). The wells also needed to be located far enough from one another that each would be contained within a unique pixel with regard to Landsat satellite imagery. This provides the opportunity to address spatial variability in ET signal with regard to vegetation cover at the site, and to address associated potential differences in drawdown magnitude with vegetation cover and distance from the river boundary. In-well transducers were employed in the wells logging water levels and water temperature at 15 or 30 minute intervals from April to November, 2009. These data will be used to validate the analytical solution or improve aquifer parameter estimation. Analysis of well hydrographs (White, 1932) can also be used as a check for ET calculations (Figure 2.1).

Chapter 4

RESULTS

In this chapter, results are presented for daily ET calculations based on temperature, radiation, and vegetation measurements at the site (or near-site). Hydrographs from in-well transducers are shown and compared to analytically modeled drawdown based on known aquifer parameters and daily ET flux.

4.1 Daily Evapotranspiration

Daily evapotranspiration (ET) rates were calculated as described in Equation 3.1 for each of four Landsat 5 pixels at the BHRS that have wells used for observations in this study (outlined in Figure 4.1). Each area for which an ET flux is applied is based on the quantification of vegetation using NDVI derived from Landsat 5 data. NDVI values for the three pixels that encompass the X wells (X2, X3, X4) are generally located in areas of the BHRS that have more vegetation while C1 is located in the middle of the well field, which is largely clear of vegetation. C1 was chosen to provide contrast to the more densely vegetated areas and to see if there were observable differences in magnitude of diurnal water table fluctuations at this site.



Figure 4.1: Aerial photograph (2009 NAIP, 1 m resolution) provides the base image of the BHRS. The grid overlain on the photo represents NDVI values from July 5, 2009 Landsat 5 data. Each grid cell represents a 30x30m pixel (spatial resolution of the satellite data) and is plotted here in grayscale with lighter squares representing higher NDVI values (more dense vegetation) and darker squares representing lower NDVI.

Figure 4.1 also shows the position of the wells and the corresponding areas for which NDVI was calculated. Figure 4.2 displays the calculated ET amplitude (mm/day) at each of the four wells for the monitoring period. It is assumed that net radiation and temperature are uniform across these four pixels (60m x 60m area) so the daily differences in calculated ET amplitude between the wells correspond to the vegetation cover at each well. [See appendix for calculated daily ET at the four wells.]

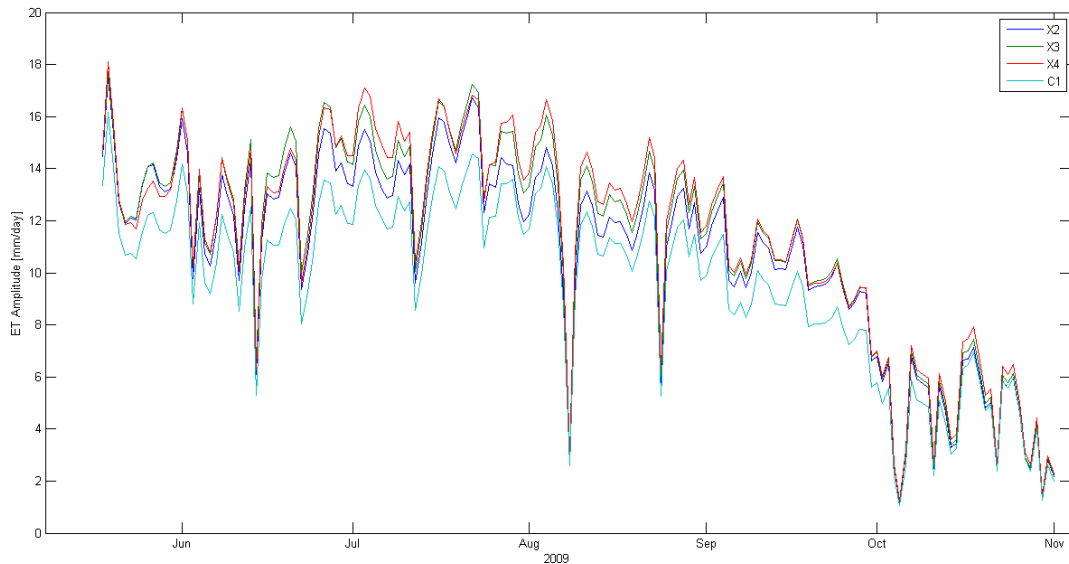


Figure 4.2: ET amplitude from mid-May through October in 2009 at the BHRS for four wells. The X labeled wells are located in more densely vegetated areas (see Figure 4.1) and well C1 is located in the central well field that is noticeably more void of vegetation. Calculated ET amplitudes reflect this difference in vegetation cover.

ET amplitude (Q in Equation 2.8) is the maximum ET flux during the day occurring at the midpoint of t_{day} . The cumulative daily ET can be found through the integration of Equation 2.8 over the period of t_{day} . Average values of ET amplitude and total ET for the period between May 18-September 1 in 2009 are listed in Table 4.1.

	ET Amplitude [mm/day]	Cumulative ET [mm/day]
X2	12.93	5.09
X3	13.61	5.35
X4	13.72	5.40
C1	11.65	4.58

Table 4.1: Average maximum and cumulative ET rates at four BHRS wells from May 18-September 1, 2009.

Locally, ET is calculated as a function of vegetation (NDVI), mean air temperature, and net radiation. As described more thoroughly in previous sections, the small size of the site allows for the assumption that net radiation and air temperatures are the same at each well. Therefore, the only variable for ET that changes between wells is the one relating to vegetation (NDVI). ET will first be analyzed as change over the summer of 2009. This discussion will look into the effect of changes in mean air temperature and net radiation over the year. Also included will be discussion of major trends in NDVI at the BHRS as a whole over the summer. Once change in time has been characterized, spatial heterogeneity will be discussed.

4.1.1 Seasonal Variation in ET signal

To examine temporal variation in the ET signal at the BHRS, graphics and discussion in this section will be limited to one well (X2) with a single set of NDVI values. Figure 4.3 shows calculated ET at well X2 with daily net radiation values ($R_{n,max}$) superimposed. This balance of incoming and outgoing radiation is, as expected, highest from late spring through summer (average of $675 \text{ W}/m^2$ from May 18-Aug 1) and decreases at a progres-

sively greater rate from the beginning of August. Observed daily variation in $R_{n,max}$ is

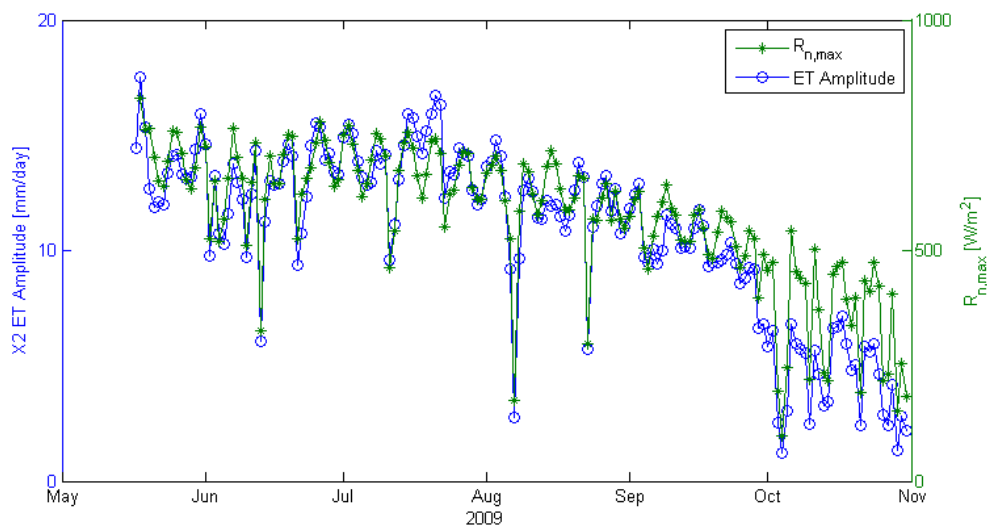


Figure 4.3: ET amplitude [mm/day] from May 18 - November 1 at well X2 plotted against daily $R_{n,max}$; these $R_{n,max}$ values were used to calculate daily ET flux.

typically less than 50 W/m^2 , but daily changes greater than 200 W/m^2 can be seen in the data and are coincident with storm or precipitation events that increase cloud cover and cause decreases in the net radiation surplus.

Figure 4.4 plots calculated ET at X2 with time against daily average air temperature at the BHRS. Mean temperature during the 4 months from the beginning of data on May 18 to September 18 (just before first freeze and declining daily temperatures) is $21.2 \text{ }^\circ\text{C}$ with a standard deviation of $3.7 \text{ }^\circ\text{C}$.

Figure 4.5 depicts general trends in parameters used for calculating ET and compares ET amplitude and NDVI. NDVI is generally noisy during the early part of the year (May-

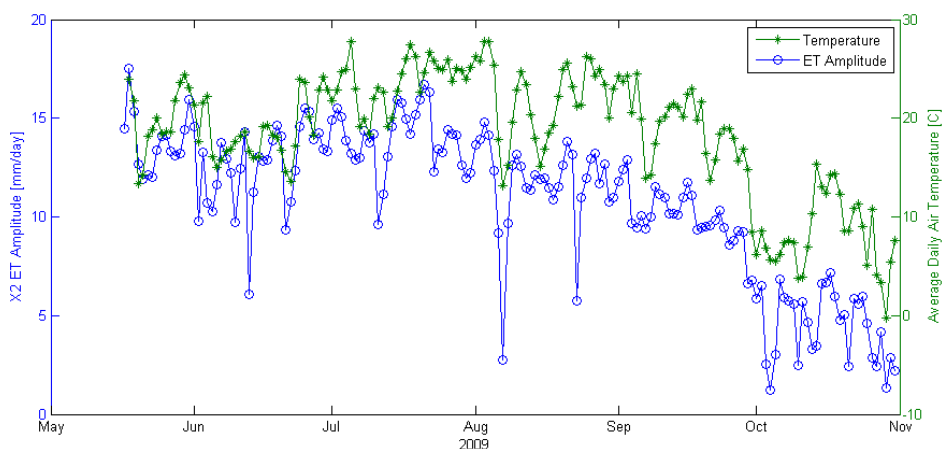


Figure 4.4: ET amplitude [mm/day] from May 18 - November 1 at well X2 plotted against daily average air temperature [$^{\circ}\text{C}$] at the BHRS that were used to calculate daily ET flux.

August) but markedly higher in magnitude with a decrease occurring in late September that continues through fall and winter. Note that NDVI was only calculated on days when Landsat 5 data were available, and NDVI was linearly interpolated between days when data were not available.

4.2 Daily Drawdown versus ET Magnitude across the Site

The diurnal signal of drawdown varies in magnitude in response to ET but is also controlled by the distance of a given well from the river. The Boise River discharge is calculated from the release rate below Lucky Peak Dam minus the diversions from Diversion Dam into the New York Canal. These data are recorded by the Bureau of Reclamation and, when paired with historical site measurements of river stage, a rating curve was developed to get river stage height as a function of discharge. Knowing the stage height also allows for an estimation of the position of the river edge at the BHRS, which provides the distance-to-

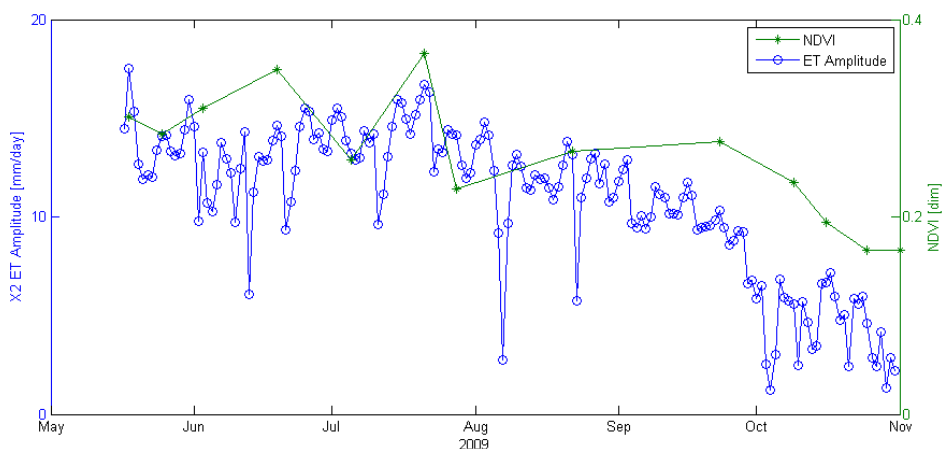


Figure 4.5: ET amplitude [mm/day] from May 18 - November 1 at well X2 plotted against calculated NDVI [-] from Landsat data at the BHRS that were used to calculate daily ET flux. Points on the NDVI line indicate values retrieved from Landsat images while the lines connecting points are linear interpolations for days with no satellite overpass.

river measurement (x in Figure 2.3) for modeling the river contributions to drawdown from ET forcing at a given location.

For comparison, daily drawdown is quantified as the maximum change in water level at a well during a day. This is not synonymous with the storage term in White (1932) but is an instantaneous measure of maximum drawdown experienced for any one day. Well hydrographs at the BHRS during periods of ET forcing typically show high daily water levels during the early morning hours (2:00-7:00) followed by drawdown during the hours where radiation is positive, resulting in maximum drawdown around 19:30, followed by a steep recovery overnight. Water levels typically do not return to the same level as the previous day. This amount of water (δS) is the residual drawdown between two maxima and the storage term from White (1932). Figure 4.6 shows a well hydrograph from well X2

in early July, 2009.

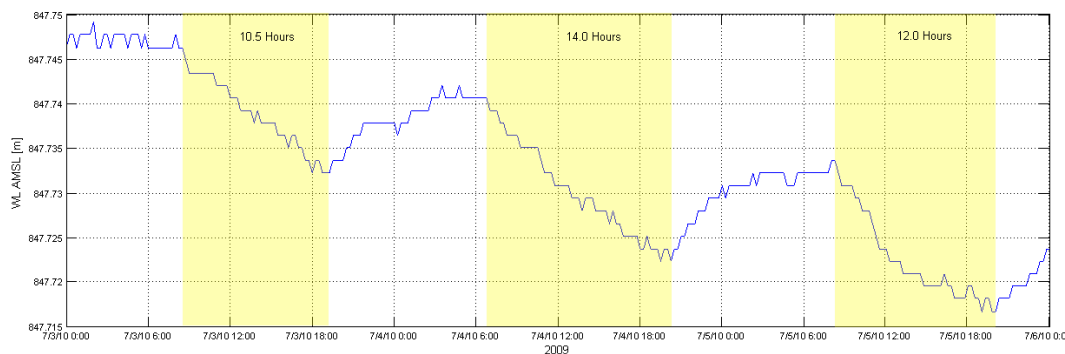


Figure 4.6: Well hydrograph from July 3-July 6, 2009 showing diurnal fluctuations of the water table in response to evapotranspiration at the BHRS at well X2. Periods of drawdown are shaded yellow with the associated length of time displayed on the graph

At equal distance (x) from the river, well drawdown magnitude should be strongly correlated with ET magnitude. The wells monitored at the BHRS are at different distances from the river edge and these differences are apparent in the well hydrographs. Figure 4.7 plots ET amplitude and daily drawdown in wells at the BHRS over different periods of time.

As shown in Figure 4.7A, X4 has the highest calculated ET amplitude for the majority of the year, followed by wells X3, X2, and C1, respectively. This order is evident from Figure 3.4 where this order is seen in the NDVI values and, keeping to the assumption that radiation and temperature are the same at each well, vegetation should be the only difference in calculating ET. The daily drawdown magnitudes in Figure 4.7B show a reversal from what is expected if distance to river was not considered. Well X4, which has the highest calculated ET values, typically has the lowest drawdown magnitudes, while well X2 has the highest drawdown values. While the absolute distance changes over the year, well X4

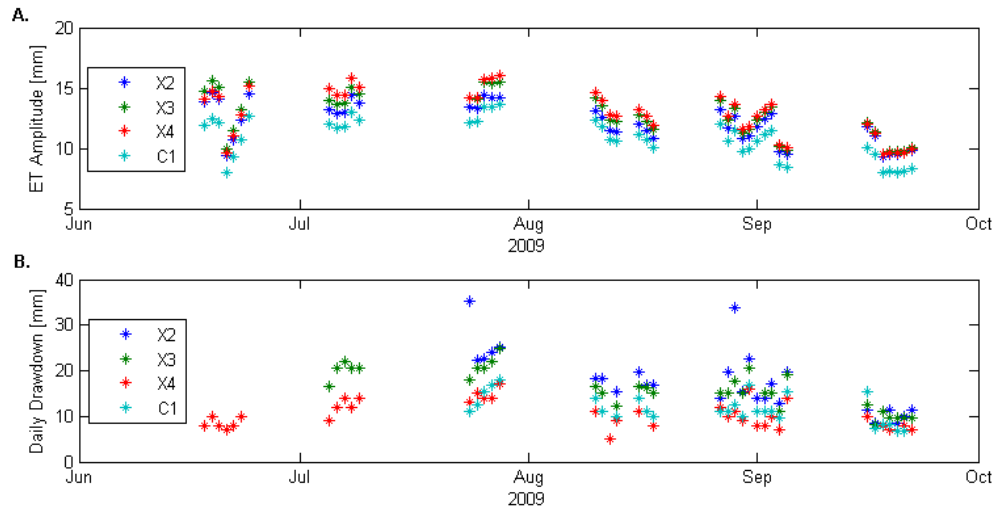


Figure 4.7: ET amplitude (A) versus well drawdown (B) over the year for four wells at the BHRS. Although X4 has the highest calculated ET rates, daily drawdown is consistently lower than the other wells due to its proximity to the river.

is always located closest to the river while X2 is always furthest away. For example, Table 4.2 shows the absolute differences in positions of the wells to the river edge in early July.

Well	Distance to River [m]
X2	82.23
C1	61.23
X3	52.55
X4	35.76

Table 4.2: Distance from wells to the river July 3, 2009.

4.3 ET_g from White (1932)

Evapotranspiration was also calculated after White (1932) from well hydrographs (Figure 2.1). ET calculated in this way is a measure of groundwater contributions (thus, it is often written as ET_g) as the aquifer is known to be coarse in grain size and shallow where vegetation can access the water and the unsaturated zone does not contribute significant amounts of water. Although wells in White (1932) are located in the riparian zone, there is no mention of the distance each well is located away from the river or stream. This, as shown in the analytical solution to drawdown, can be problematic as drawdown magnitude is a function of lateral distance from the river boundary. Wells X4 and X2 represent wells closest and furthest away, respectively, from the river boundary (Table 4.2). Figures 4.8 and 4.9 show ET calculated using the White (1932) method and the radiation-based model from Batra *et al.* (2006).

Good agreement is seen between the methods at well X4, which is closest to the river boundary. ET from White (1932) at well X2 is consistently higher than what is calculated through the radiation-based method with values being 60% higher for three of the days presented in Figure 4.8.

4.4 Modeled Drawdown

Drawdown can be solved for analytically with a known daily ET flux, river edge position, and hydraulic conductivity and aquifer storage parameters. Modeled drawdown with known flow system parameters here will further support the findings that daily ET functions are accurate and assumptions inherent in the models used are valid. Modeled drawdown here accounts for both differences in lateral position and daily ET flux. Figures 4.10 and

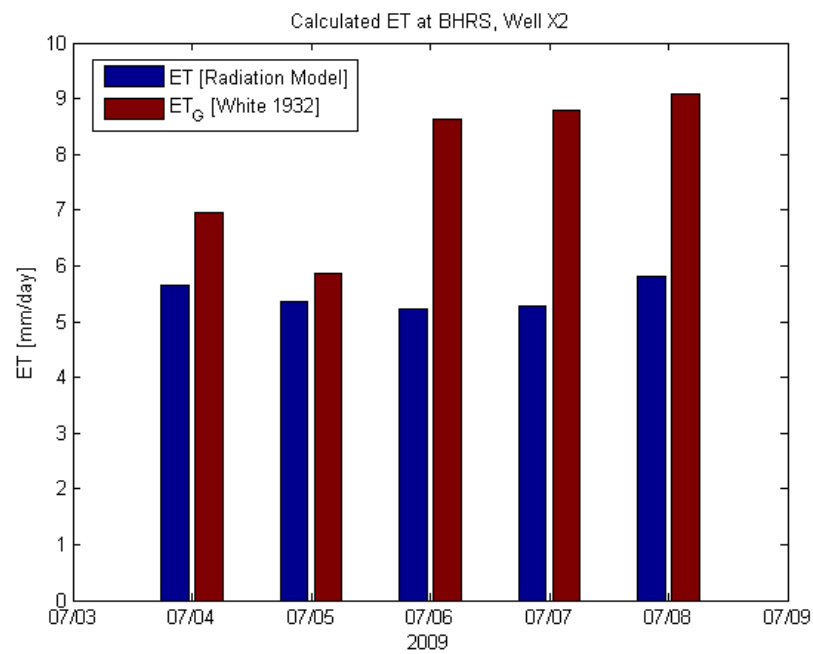


Figure 4.8: Results of ET calculated at well X2 over 5 days using the radiation based method from Batra *et al.* (2006) compared to ET calculated from well hydrographs (White, 1932)

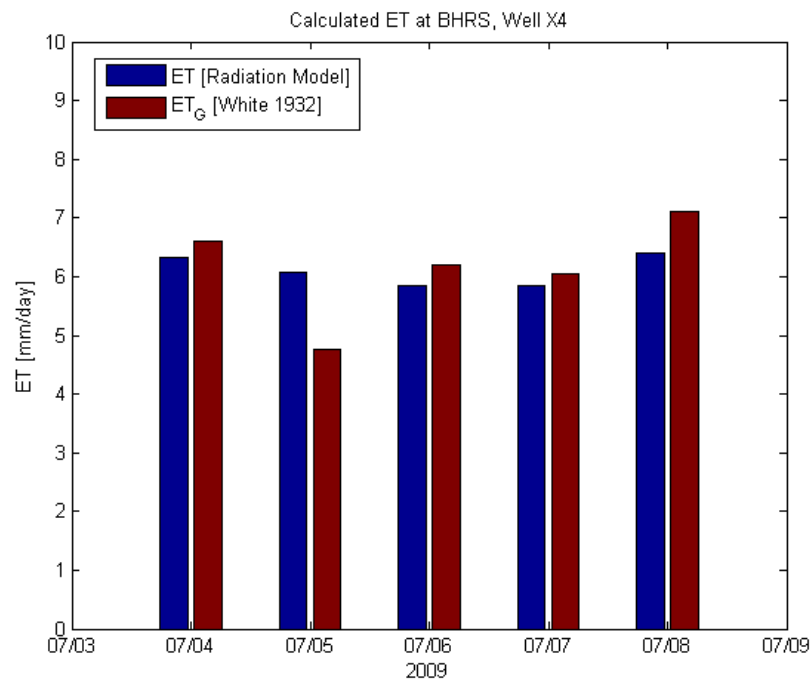


Figure 4.9: Results of ET calculated at well X4 over 5 days using the radiation based method from Batra *et al.* (2006) compared to ET calculated from well hydrographs (White, 1932)

4.11 show modeled response to changes in the lateral position from the river edge and ET flux applied at the water table, respectively. As seen in Figure 4.10, daily drawdown magnitude increases as the distance between the river edge and the observation well increases.

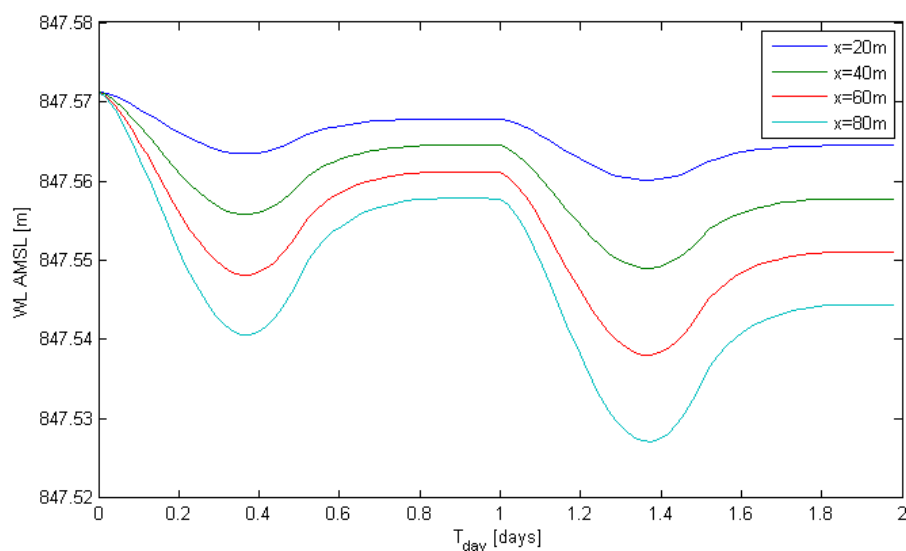


Figure 4.10: Modeled water table elevation at the well with increasing distance from the river edge. Aquifer conductivity and ET flux are held constant and the distance between the well and river edge [x] is changed for each model run.

Good agreement between observed and modeled drawdown in Figure 4.12 supports the timing and magnitude of calculated ET flux as applied to the observed drawdown data at the BHRS. Successful demonstration of this modeled relationship supports further use of the analytical solution (Malama & Johnson, 2010) to solve for hydraulic conductivity if drawdown records are available (see Chapter 5).

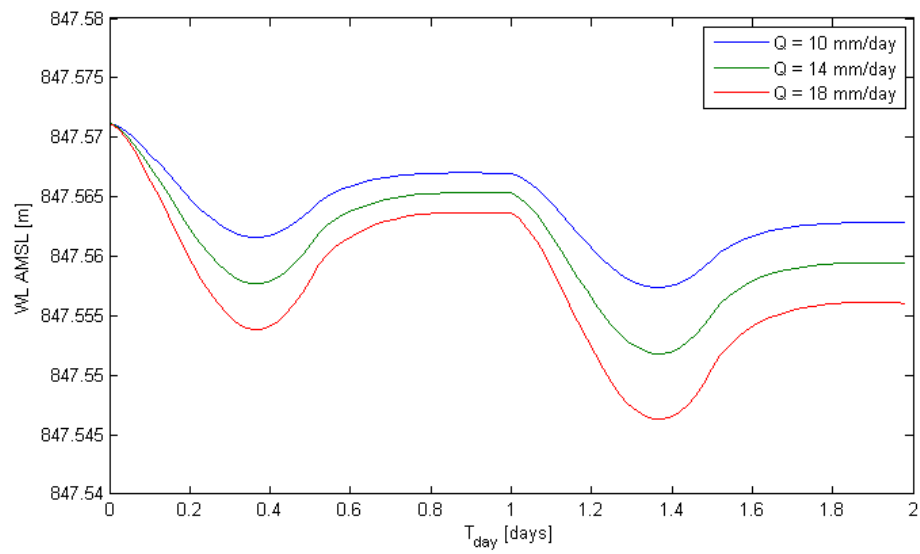


Figure 4.11: Modeled water table elevation at the well with increasing ET amplitude [Q]. Aquifer conductivity and the distance from the river edge are held constant and the ET flux is changed for each model run.

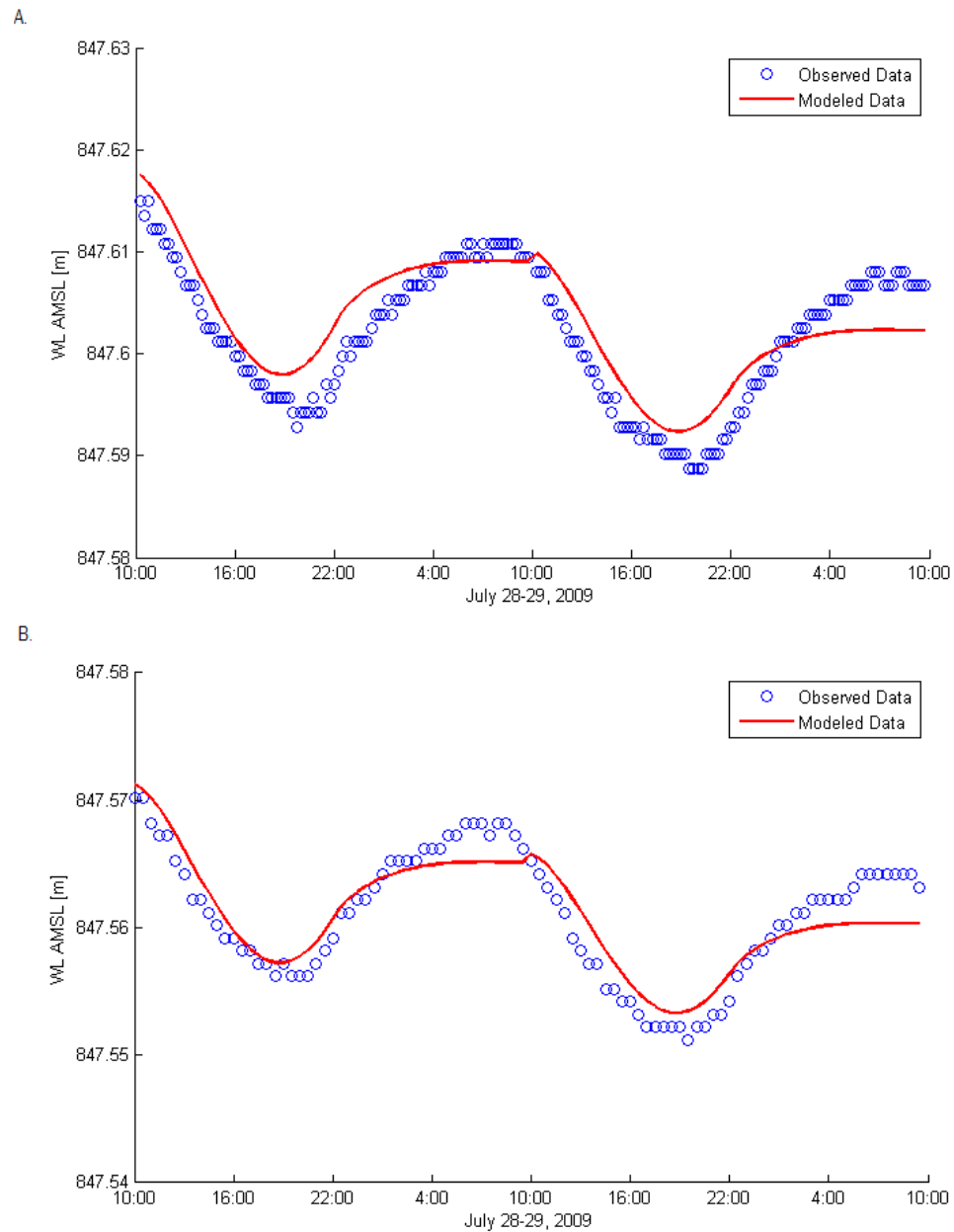


Figure 4.12: Modeled water table elevation versus observed (A) at well X3 and (B) at well X4 in July, 2009. Modeled results here use average aquifer hydraulic conductivity values defined in Table 1.1, and river edge distances (x) of 53m and 36m, respectively.

Chapter 5

DISCUSSION

This chapter includes the results and discussion of a sensitivity analysis of the parameters used to calculate ET and correlations between the parameters at calculated ET. Spatial variations in vegetation and net radiation are discussed as they relate to ET calculations at the BHRS. Finally, analytically modeled drawdown is presented and fit to observed data through the optimization of hydraulic conductivity values.

5.1 Parameter Sensitivity Analysis

This analysis will investigate and quantify uncertainties in calculated ET given assumed uncertainties in the measurements required as input to the ET model. The parameter sensitivity analysis was conducted by first determining the average values for air temperature, net radiation, and NDVI from May 18-August 1, 2009. The trend in parameters over this time period is relatively constant (Figures 4.3, 4.4, and 4.5) and this allows for a simple estimate of average ET amplitude over the time period, which agrees well with a value derived from averaging daily ET amplitude values. A standard deviation of error was determined for each of the three parameters and a Monte Carlo simulation was performed to

quantify the likely uncertainty associated with each parameter.

It is assumed that from June-August vegetation should be at its greatest extent and should be at steady state with regard to NDVI. Standard deviation of the Landsat-derived NDVI measurements from this time is 0.028 [dim]. A standard deviation of 4 [W/m^2] is used to describe variability in $R_{n,max}$ and is based on observations seen in the instantaneous estimates from multiple net radiometers by Blonquist *et al.* (2007). Blonquist *et al.* (2007) do report a bias of +8% in predicting net radiation from solar radiation and common weather data, which could lead to overestimation of ET. A standard deviation of 0.2 °C is used for air temperature and is equal to the resolution of the temperature sensor at the BHRS.

Parameter sensitivity was determined through a Monte Carlo simulation using a normally distributed variable sample with standard deviations equal to the values described above. The results are shown in Figure 5.1. From this simulation, as the variance increases between maximum and minimum seasonal ET, more uncertainty is associated with each parameter. The standard deviations of mean ET calculations are displayed in Table 5.1. The error presented here relates only to sensor and measurement errors and does not consider spatial variations or error as the result of assumptions made in the calculation of ET.

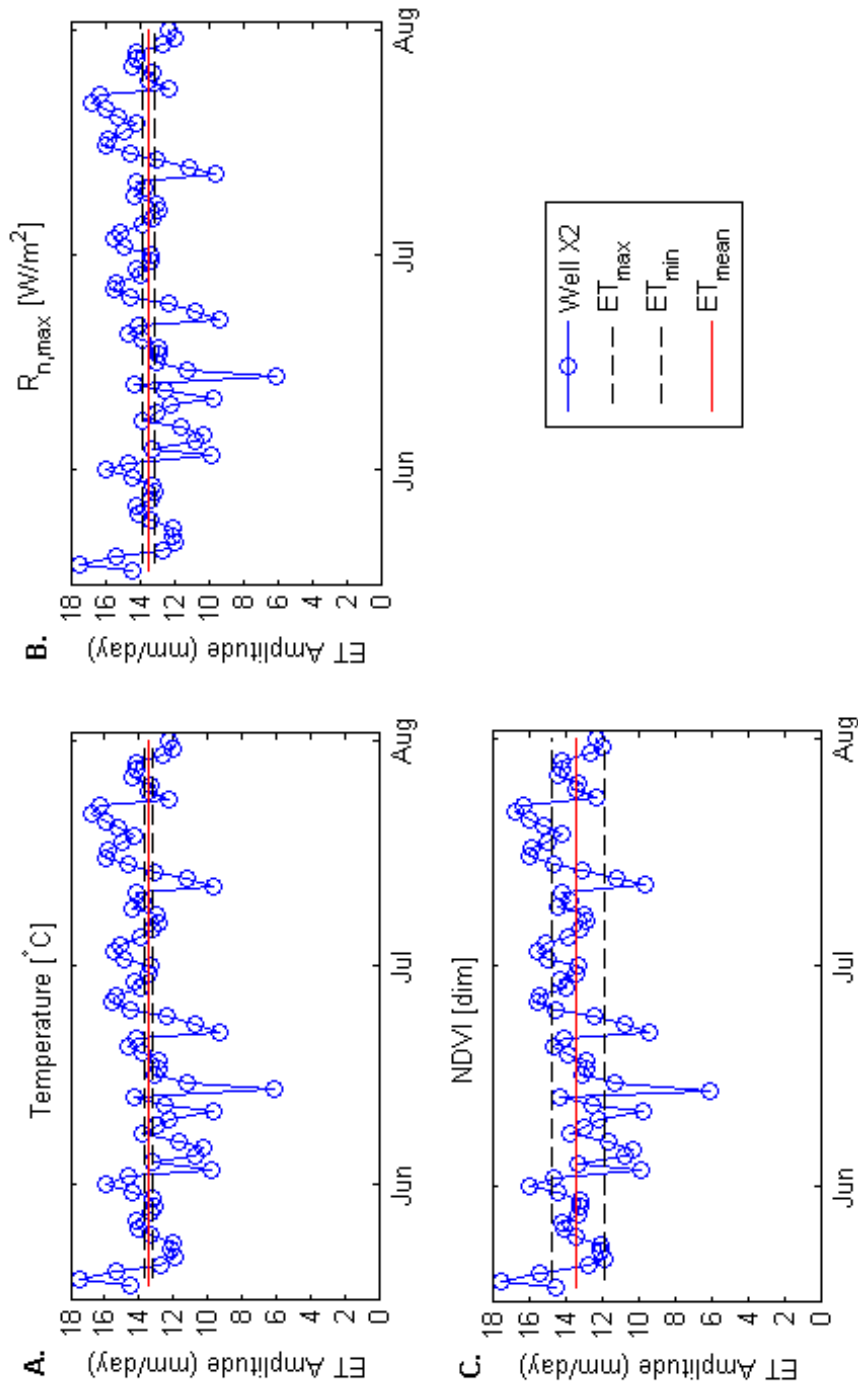


Figure 5.1: ET amplitude at X2 from May 18-August 1, 2009 plotted with results of Monte Carlo simulation for parameter sensitivity analysis for (A) temperature, (B) net radiation, and (C) NDVI. Seasonal mean ET amplitude (13.44 mm/day) is shown as the red line bounded by maximum and minimum average values for seasonal ET as a result of the simulation.

	ET Standard Deviation	Units	Q Amplitude Error [mm/day]
T	0.053	$^{\circ}\text{C}$	0.46
$R_{n,max}$	0.080	W/m^2	0.65
NDVI	0.35	dim	2.91

Table 5.1: Results from parameter sensitivity simulation for mean ET values in response to variation in each parameter at well X2.

The results of the simulation show that the greatest uncertainty is associated with vegetation quantification through NDVI. The standard deviation used for NDVI measurements was based on the assumption that vegetation density was at steady state from June-August and any changes seen at a pixel in NDVI were a product of retrieval uncertainty. This uncertainty would be best addressed by periodic ground truthing of vegetation by measuring plant-scale reflectance or leaf area index (LAI). Although empirical relationships between NDVI and LAI can be made, relationships are dependent on the phenological stages of the vegetation and the relationship during the period of maximum vegetation extent is not well quantified (Wang *et al.*, 1995). Even with the ambiguities presented for NDVI during this period, relative NDVI rankings between pixels should not be affected because much of the noise can be attributed to background reflection differences (Wang *et al.*, 1995), which are similarly sensed over the entire area.

The cited bias associated with net radiation estimates from solar radiation (Blonquist *et al.*, 2007) is within the uncertainty presented in this analysis and is not considered to be problematic for ET calculations when compared to the error associated with net radiation from satellite retrieval (Bisht *et al.*, 2005).

5.2 ET Parameter Correlation

ET was calculated using a radiation-based method with additional considerations for vegetation (NDVI) and air temperature. Figure 5.2 shows the results of regression analysis between the three parameters and calculated ET amplitude from May 18-September 1, 2009 at the BHRS at well X2. ET calculations are based on Priestley & Taylor (1972), which is a radiation-based method and, as expected, correlation is strongest with maximum daily net radiation.

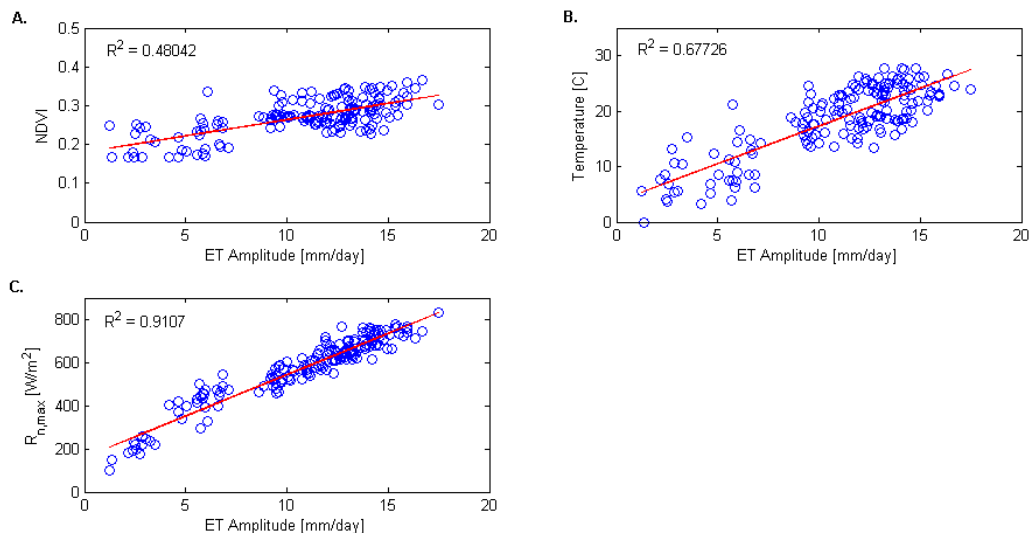


Figure 5.2: Regression analysis for calculated ET amplitude versus net radiation, NDVI, and average air temperature for dates May 18-September 1 2009

5.3 Spatial Variation in ET Signal

As previously discussed, air temperature measurements were made at the BHRS and applied uniformly over the entire site. Net Radiation values were derived from an AgriMet

weather station in the vicinity of the site and these data were applied uniformly at the site. From an energy balance standpoint, soil heat flux is not calculated directly but is determined through a relationship with NDVI and $R_{n,max}$ in Equation 2.5 (Batra *et al.*, 2006; Moran *et al.*, 1989). Here, a single $R_{n,max}$ value is used across the site but vegetation cover in the ET calculation will dictate the amount of radiation applied at the pixel level. Higher NDVI values mean more vegetation and less energy at the ground surface resulting in lower soil heat flux values with more radiation going to the vegetation resulting in higher ET. Low vegetation cover (and NDVI) results in more energy hitting the ground surface, which increases soil heating.

It follows that for any given day, vegetation density (NDVI) is the only parameter that differentiates the calculated ET flux from each well. Values for NDVI at each well can be seen in Table 3.1 and Figure 3.4. These values are applied to every well contained within a Landsat pixel for which NDVI is calculated. Figure 4.1 shows the wells for which water levels were monitored and shows the area over which the NDVI value is calculated and the ET flux is applied.

It is apparent from Figure 4.1 that vegetation is not homogeneous within a pixel. No attempts to remedy the mixed pixel issue were attempted. However, NDVI is a proxy for vegetation cover in the area so spatial differences at the wells are observed at a 30m resolution. Inspection of the photograph coupled with on-site visual observations confirm that the X wells are surrounded by more vegetation than C1 and higher NDVI values would be expected at the X wells. Figure 5.3 depicts how NDVI values affect both instantaneous and cumulative ET flux. The range in NDVI (0.1-0.5) bounds the observed set of values at the

BHRS in 2009. The ET rates calculated in Figure 5.3 use $R_{n,max}$ of 700 W/m^2 and average air temperature of $25 \text{ }^\circ\text{C}$. Over this NDVI range, Q (peak ET flux rate) ranges from 11.45 mm/day to 17.30 mm/day which corresponds to a difference of 2.32 mm/day in cumulative daily ET over a particular area.

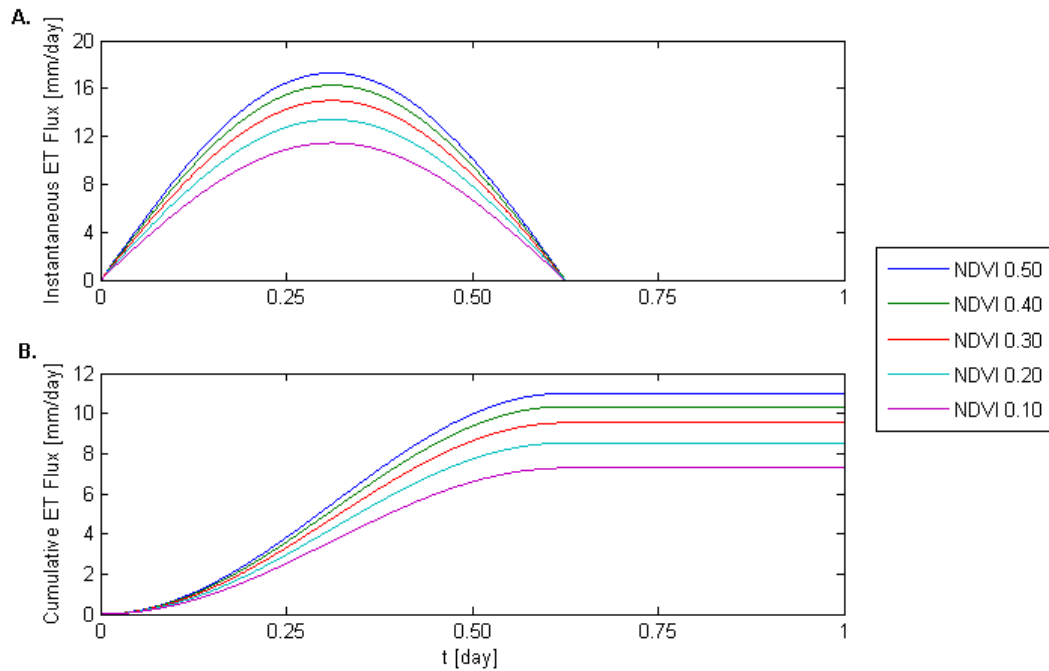


Figure 5.3: (A) Instantaneous ET flux [mm/day] during a 24 hour period ($t = 1$). For this example t_{day} , time over which $f(t)$ is applied, is equal to 0.625 (15 hours). The amplitude of the curve is equal to the reported Q values for ET. (B) Cumulative ET flux [mm] over a 24 hour period.

5.4 Analytical Drawdown Model

Selected days over summer 2009 were chosen to test the analytical model of Malama & Johnson (2010) for predicted drawdown in response to ET flux. Criteria for selection include the following factors:

1. Constant river stage for two days prior,
2. Head observations available from in-well transducers,
3. Clear sky days with high net radiation values,
4. Proximity to measured NDVI value.

These criteria help with comparing model results both to observed data for the day and to previous modeled results from different times of the year. The criteria were also used in the forward modeling of drawdown due to ET discussed in Section 4.3. River stage head fluctuations can be modeled through the analytical solution of Malama & Johnson (2010), but magnitude of the change in river stage typically results in water level changes an order of magnitude higher than that of the diurnal fluctuations of the water level caused by ET. For this reason, days immediately after river changes are ignored because aquifer water levels have not yet equilibrated with river levels.

It is also preferable to have days close to a measured NDVI value. Although NDVI has been determined for every day from summer 2009, days in between Landsat-derived NDVI were linearly interpolated. The change in NDVI at each well is small over the data record and linear interpolations are generally only for one or two week periods, depending on satellite availability. Clear sky days with high (positive) net radiation values are com-

mon and are preferred because of the strong ET signal that results due to higher radiation. Generally speaking, this also limits effects of precipitation in water use for the analytical model that assumes unsaturated zone water contribution as negligible.

The results of the modeled drawdown with optimized hydraulic conductivity values presented in Figure 4.12 show that if the aquifer system is well defined and ET is known, drawdown can be solved for a given period of time. Here, the inverse solution is presented by using the same ET flux at the water table with a record of well water levels and solving for hydraulic conductivity (horizontal (K_x) and vertical (K_z)) at a known distance from the river edge (x). The conductivity values presented in Figure 5.4 are the result of a least squares optimization of K_x and K_z given a set of observed well water levels and calculated ET.

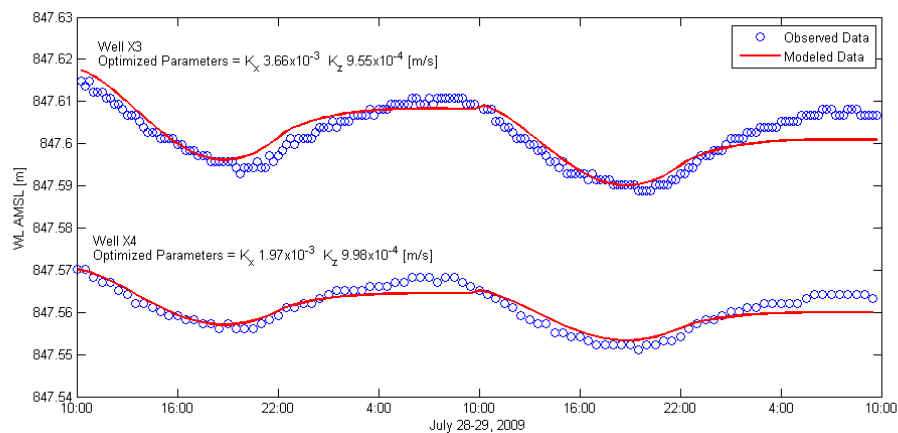


Figure 5.4: Using calculated ET and water records from in-well transducers, along with aquifer system parameters such as distance from river and saturated aquifer thickness, hydraulic conductivity is estimated using a least squares optimization.

Parameter	Values from Fox (2006)			Optimized
	Mean	Maximum	Minimum	Mean
K_x	7.59×10^{-4}	1.29×10^{-3}	5.13×10^{-4}	2.82×10^{-3}
K_z	6.61×10^{-4}	1.29×10^{-3}	3.80×10^{-5}	9.77×10^{-4}

Table 5.2: Range and mean of hydraulic conductivity values from pumping tests at the BHRS (Fox, 2006) and mean values from well X3 and X4 through the inversion of draw-down records using the analytical model of Malama & Johnson (2010)

Hydraulic conductivity values determined through this routine generally agree with previous values derived from pumping tests (Fox, 2006) and slug tests. Values for storage properties have not been a part of the optimization due to difficulties with the low values noted at the site previously (Barrash *et al.*, 2006) and have been attributed to analytical solutions for drawdown over relatively short periods of time (Neuman, 1972).

Chapter 6

SUMMARY AND CONCLUSIONS

The main focus of this study was to characterize and quantify the daily evapotranspiration signal at the BHRS. A hybrid approach was used to calculate ET using local meteorological data and remotely sensed vegetation parameters from Landsat 5 satellite data. A daily model of ET flux was created and applied at four distinct Landsat pixels that included four wells at the BHRS. This same methodology could be scaled up to encompass the entirety of the BHRS and all saturated zone installations. With ET defined at the site, daily drawdown was modeled using the analytical solution of Malama & Johnson (2010). Hydraulic conductivity data from previous aquifer tests were used for aquifer parameters and a river rating curve for stage height was used to determine the lateral distance between the river and well during the year. These parameters, when coupled with daily ET flux, provided the necessary information to forward model drawdown in the wells. Observed drawdown showed good agreement with modeled drawdown, which suggests that both aquifer parameters and ET magnitude are well characterized at the site.

Analytical modeling of drawdown due to ET has also provided insight to relative water contributions of the aquifer and river to vegetation demands. Although ET magnitude

is a control on drawdown at the wells, the distance between the well and the river edge plays a vital part in the magnitude of drawdown observed at the well. This relationship was successfully modeled and future work is planned to further quantify relative water source contributions.

With ET and the aquifer system well characterized, an inverse solution was investigated by fitting modeled drawdown to observed data by optimizing aquifer parameters (K_x and K_z) using a least squares fit approach. This work resulted in the successful determination of conductivity values from in-well transducers and a well-characterized daily ET flux.

REFERENCES

- Allen, R. G., Pereira, L. S., Raes, D., & Smith, M. 1998. *Crop evapotranspiration - Guidelines for computing crop water requirements*. FAO Irrigation and Drainage Papers 56. Food and Agriculture Organization.
- Barrash, W., & Clemo, T. 2002. Hierarchical geostatistics and multifacies systems: Boise Hydrogeophysical Research Site, Boise, Idaho. *Water Resources Research*, **38**(10), 1196. doi:10.1029/2002WR001436.
- Barrash, W., Clemo, T., Hyndman, D., Reboulet, E., & Hausrath, E. 2002. *Tracer/Time-Lapse Radar Imaging Test; Design, Operation, and Preliminary Results*. Tech. rept. Boise State University.
- Barrash, W., Clemo, T., Fox, J. J., & Johnson, T. C. 2006. Field, laboratory, and modeling investigation of the skin effect at wells with slotted casing. *Journal of Hydrology*, **326**(1–4), 181–198. doi:10.1016/j.jhydrol.2005.10.029.
- Batra, N., Islam, S., Venturini, V., Bisht, G., & Jiang, L. 2006. Estimation and comparison of evapotranspiration from MODIS and AVHRR sensors for clear sky days over the Southern Great Plains. *Remote Sensing of Environment*, **103**, 1–15.

- Beschta, R. L. 2005. Reduced cottonwood recruitment following expiration of wolves in Yellowstone's northern range. *Ecology*, **86**(2), 391–403.
- Bisht, G., Venturini, V., Jiang, L., & Islam, S. 2005. Estimation of the net radiation using MODIS (moderate resolution imaging spectro-radiometer) data for clear sky days. *Remote Sensing of Environment*, **97**, 52–67.
- Blonquist, M, Tanner, B., & Bugbee, B. 2007. *Evaluation of two new net radiometers and a model to predict net radiation*. Tech. rept. Apogee Instruments, Inc. and Campbell Scientific, Inc.
- Butler Jr., J. J., Kluitenberg, G. J., Whittemore, D. O., Lodeide II, S. P., Jin, W., Billinger, M. .A., & Zhan, X. 2007. A field investigation of phreatophyte-induced fluctuations of the water table. *Water Resources Research*, **43**, W02404, doi:10.1029/2005WR004627.
- Cardiff, M., Barrash, W., Kitanidis, P.K., Malama, B., Revil, A., Straface, S., & Rizzo, E. 2009. A potential-based inversion of unconfined steady-state hydraulic tomography. *Ground Water*, **47**(2), 259–270.
- Dingman, S. L. 2002. *Physical Hydrology*. Prentice Hall Inc.
- Eichinger, W. E., Parlange, M. B., & Stricker, H. 1996. On the concept of equilibrium evaporation and the value of the Priestley-Taylor coefficient. *Water Resources Research*, **32**(1), 161–164.
- ENVI. 2006. *ENVI Reference Guide Version 4.3*. July 2006 edn. ITT Visual Information Solutions.

- Fox, J. J. 2006. *Analytical modeling of fully penetrating pumping tests at the Boise Hydrogeophysical Research Site for aquifer parameters and wellbore skin*. M.S. Thesis, Boise State University.
- Goodrich, D. C., Scott, R., Qi, J., Goff, B., Unkrich, C. L., Moran, M. S., Williams, D., Schaeffer, S., Snyder, K., MacNish, R., Maddock, T., Pool, D., Chehbouni, A., Cooper, D. I., Eichinger, W. E., Shuttleworth, W. J., Kerr, Y., Marsett, R., & Ni, W. 2000. Seasonal estimates of the riparian evapotranspiration using remote and in situ measurements. *Agricultural and Forest Meteorology*, **105**, 281–309.
- Gribovszki, Z., Kalicz, P., Szilágyi, J., & Kucsara, M. 2008. Riparian zone evapotranspiration estimation from diurnal groundwater level fluctuations. *Journal of Hydrology*, **349**, 6–17.
- Hipps, L., Cooper, D., Eichinger, W., Williams, D., Schaeffer, S., Snyder, K., Scott, R., Chehbouni, A., Watts, C., Hartogensis, O., Lhomme, J. P., Monteny, B., Brunel, J. P., Boulet, G., Schieldge, J., de Bruin, H., Shuttleworth, J., & Kerr, Y. 1998. A summary of processes which are connected to evaporation of riparian and heterogeneous upland vegetation in arid regions. *Proceedings of the Special Symposium of American Society of Meteorologists on Hydrology*.
- Jiang, L., & Islam, S. 2001. Estimation of surface evaporation map over southern Great Plains using remote sensing data. *Water Resources Research*, **37**(2), 329–340.
- Liang, S. 2004. *Quantitative remote sensing of land surfaces*. Vol. One. New Jersey: John Wiley & Sons, Inc.

- Loheide II, S. P. 2008. A method for estimating subdaily evapotranspiration of shallow groundwater using diurnal water table fluctuations. *Ecohydrology*.
- Loheide II, S. P., Butler Jr., J. J., & Gorelick, S. M. 2005. Estimation of groundwater consumption by phreatophytes using diurnal watertable fluctuations: A saturated-unsaturated flow assessment. *Water Resources Research*, **41**, W07030, doi:10.129/2005WR003942.
- Malama, B., & Johnson, B. 2010. Analytical modeling of saturated zone head response to evapotranspiration and river-stage fluctuations. *Journal of Hydrology*, **382**, 1–9. doi:10.1016/j.jhydrol.2009.12.010.
- Meyboom, P. 1967. Groundwater studies in the Assiniboine River drainage basin-Part II: Hydrologic characteristics of phreatophytic vegetation in south-central Saskatchewan. *Bulletins of Geological Survey of Canada*.
- Moran, M. S., Jackson, R. D., Raymond, L. H., Gay, L. W., & Slater, P. N. 1989. Mapping surface energy balance components by combining landsat thematic mapper and ground-based meteorological data. *Remote Sensing of Environment*, **30**, 77–87.
- Neuman, S. P. 1972. Theory of flow in unconfined aquifers considering delayed response of the water table. *Water Resources Research*, **8**(4), 1031–1045.
- Price, J. C. 1987. Calibration of satellite radiometers and comparison of vegetation indices. *Remote Sensing of Environment*, **14**, 35–48.
- Priestley, C. H. B., & Taylor, R. J. 1972. On the assessment of surface heat flux and evaporation using large-scale parameters. *Monthly Weather Review*, **100**(2), 81–91.

- Shah, N., Nachabe, M., & Ross, M. 2007. Extinction depth and evapotranspiration from ground water under selected land covers. *Ground Water*, **45**(3), 329–338.
- Troxel, H. C. 1936. The diurnal fluctuation in the groundwater and flow of the Santa Ana river and its meaning. *EOS Transactions*.
- Tso, B., & Mather, P. 2009. *Classification methods for remotely sensed data*. CRC Press.
- Wang, Q., Adiku, S., Tenhunen, J., & Granier, A. 1995. On the relationship of NDVI with leaf area index in a deciduous forest site. *Remote Sensing of Environment*.
- White, W. N. 1932. *A method for estimating ground-water supplies based on discharge by plants and evaporation from soil – Results of investigations in the Escalante Valley, Utah*. Tech. rept. 659–A. USGS.

Appendix A

ET AMPLITUDE FOR WELLS, 2009

Date	X2_amp	X3_amp	X4_amp	C1_amp
05/17/09	14.46	14.64	14.64	13.36
05/18/09	17.51	17.73	18.11	16.18
05/19/09	15.36	15.53	15.71	14.08
05/20/09	12.68	12.80	12.82	11.50
05/21/09	11.88	11.98	11.86	10.66
05/22/09	12.10	12.17	11.92	10.73
05/23/09	12.02	12.07	11.67	10.54
05/24/09	13.37	13.41	12.79	11.58
05/25/09	14.08	14.10	13.26	12.20
05/26/09	14.13	14.21	13.52	12.30
05/27/09	13.32	13.45	12.93	11.65
05/28/09	13.12	13.30	12.92	11.52
05/29/09	13.21	13.46	13.19	11.66
05/30/09	14.39	14.71	14.54	12.75
05/31/09	15.94	16.35	16.30	14.18

06/01/09	14.60	15.04	15.10	13.05
06/02/09	09.79	10.12	10.23	08.79
06/03/09	13.25	13.74	13.98	11.94
06/04/09	10.73	11.16	11.29	09.63
06/05/09	10.28	10.71	10.79	09.19
06/06/09	11.62	12.13	12.16	10.36
06/07/09	13.77	14.41	14.38	12.24
06/08/09	12.97	13.60	13.50	11.49
06/09/09	12.21	12.83	12.68	10.78
06/10/09	09.71	10.22	10.05	08.54
06/11/09	12.48	13.16	12.89	10.94
06/12/09	14.31	15.12	14.74	12.50
06/13/09	06.09	06.44	06.25	05.30
06/14/09	11.23	11.91	11.51	09.75
06/15/09	13.03	13.84	13.31	11.27
06/16/09	12.83	13.65	13.08	11.07
06/17/09	12.88	13.72	13.09	11.07
06/18/09	13.85	14.78	14.04	11.86
06/19/09	14.61	15.62	14.78	12.48
06/20/09	14.09	15.06	14.34	12.08
06/21/09	09.35	09.98	09.57	08.04
06/22/09	10.74	11.47	11.07	09.27
06/23/09	12.34	13.17	12.80	10.69
06/24/09	14.56	15.53	15.20	12.66

06/25/09	15.53	16.56	16.33	13.56
06/26/09	15.36	16.37	16.27	13.47
06/27/09	13.91	14.82	14.83	12.25
06/28/09	14.23	15.15	15.27	12.58
06/29/09	13.41	14.27	14.50	11.91
06/30/09	13.30	14.14	14.48	11.86
07/01/09	14.89	15.82	16.33	13.34
07/02/09	15.49	16.44	17.11	13.94
07/03/09	15.09	16.01	16.80	13.64
07/04/09	13.87	14.70	15.55	12.59
07/05/09	13.20	13.98	14.92	12.05
07/06/09	12.87	13.60	14.42	11.70
07/07/09	12.99	13.69	14.43	11.76
07/08/09	14.34	15.09	15.81	12.94
07/09/09	13.76	14.45	15.05	12.38
07/10/09	14.18	14.87	15.40	12.72
07/11/09	09.60	10.04	10.34	08.58
07/12/09	11.17	11.67	11.95	09.95
07/13/09	13.05	13.61	13.86	11.60
07/14/09	14.57	15.17	15.36	12.91
07/15/09	15.94	16.58	16.69	14.08
07/16/09	15.78	16.38	16.41	13.90
07/17/09	14.94	15.48	15.43	13.12
07/18/09	14.21	14.71	14.58	12.46

07/19/09	15.19	15.70	15.48	13.28
07/20/09	15.93	16.44	16.13	13.89
07/21/09	16.71	17.23	16.82	14.56
07/22/09	16.33	16.94	16.67	14.38
07/23/09	12.29	12.84	12.74	10.96
07/24/09	13.43	14.14	14.14	12.13
07/25/09	13.29	14.11	14.24	12.17
07/26/09	14.42	15.45	15.73	13.40
07/27/09	14.19	15.35	15.79	13.41
07/28/09	14.13	15.45	16.05	13.58
07/29/09	12.64	13.80	14.34	12.13
07/30/09	11.98	13.06	13.56	11.47
07/31/09	12.24	13.33	13.84	11.70
08/01/09	13.65	14.85	15.41	13.03
08/02/09	13.90	15.10	15.67	13.24
08/03/09	14.80	16.06	16.66	14.08
08/04/09	14.12	15.29	15.87	13.40
08/05/09	12.34	13.35	13.85	11.69
08/06/09	09.19	09.93	10.30	08.70
08/07/09	02.74	02.96	03.07	02.59
08/08/09	09.67	10.42	10.80	09.12
08/09/09	12.60	13.56	14.06	11.86
08/10/09	13.14	14.13	14.64	12.35
08/11/09	12.57	13.50	13.99	11.80

08/12/09	11.45	12.28	12.72	10.72
08/13/09	11.37	12.18	12.62	10.64
08/14/09	12.14	12.99	13.45	11.34
08/15/09	11.93	12.74	13.19	11.11
08/16/09	11.98	12.78	13.23	11.14
08/17/09	11.48	12.24	12.67	10.67
08/18/09	10.85	11.54	11.95	10.06
08/19/09	11.54	12.27	12.70	10.68
08/20/09	12.63	13.42	13.88	11.68
08/21/09	13.84	14.68	15.19	12.77
08/22/09	13.17	13.95	14.43	12.13
08/23/09	05.74	06.07	06.27	05.27
08/24/09	11.00	11.63	11.99	10.08
08/25/09	11.94	12.60	12.98	10.91
08/26/09	12.92	13.62	14.01	11.77
08/27/09	13.24	13.94	14.33	12.03
08/28/09	11.69	12.30	12.62	10.59
08/29/09	12.68	13.32	13.65	11.46
08/30/09	10.76	11.29	11.56	09.70
08/31/09	11.00	11.52	11.78	09.88
09/01/09	11.81	12.36	12.61	10.58
09/02/09	12.42	12.98	13.23	11.10
09/03/09	12.88	13.45	13.69	11.48
09/04/09	09.69	10.10	10.27	08.61

09/05/09	09.48	09.87	10.01	08.39
09/06/09	10.04	10.44	10.58	08.87
09/07/09	09.42	09.79	09.90	08.30
09/08/09	10.01	10.39	10.49	08.79
09/09/09	11.53	11.95	12.05	10.10
09/10/09	11.15	11.54	11.62	09.74
09/11/09	10.96	11.33	11.39	09.54
09/12/09	10.14	10.46	10.50	08.79
09/13/09	10.15	10.47	10.49	08.78
09/14/09	10.11	10.41	10.41	08.72
09/15/09	10.99	11.29	11.28	09.44
09/16/09	11.74	12.05	12.02	10.06
09/17/09	11.07	11.35	11.30	09.46
09/18/09	09.32	09.55	09.49	07.94
09/19/09	09.47	09.69	09.61	08.04
09/20/09	09.49	09.69	09.60	08.03
09/21/09	09.58	09.77	09.66	08.08
09/22/09	09.86	10.04	09.91	08.29
09/23/09	10.35	10.53	10.38	08.68
09/24/09	09.44	09.61	09.50	07.94
09/25/09	08.59	08.75	08.67	07.23
09/26/09	08.82	08.99	08.94	07.44
09/27/09	09.27	09.45	09.44	07.84
09/28/09	09.22	09.40	09.41	07.81

09/29/09	06.62	06.75	06.78	05.62
09/30/09	06.80	06.95	07.00	05.79
10/01/09	05.83	05.96	06.02	04.97
10/02/09	06.53	06.67	06.77	05.58
10/03/09	02.55	02.60	02.65	02.18
10/04/09	01.21	01.24	01.27	01.04
10/05/09	03.05	03.12	03.20	02.62
10/06/09	06.84	07.00	07.20	05.90
10/07/09	05.93	06.07	06.27	05.12
10/08/09	05.75	05.90	06.10	04.98
10/09/09	05.58	05.73	05.95	04.85
10/10/09	02.50	02.57	02.68	02.20
10/11/09	05.68	05.86	06.13	05.09
10/12/09	04.65	04.81	05.05	04.22
10/13/09	03.28	03.40	03.59	03.03
10/14/09	03.46	03.60	03.81	03.24
10/15/09	06.65	06.93	07.36	06.31
10/16/09	06.70	07.01	07.47	06.46
10/17/09	07.14	07.46	07.94	06.92
10/18/09	05.96	06.22	06.62	05.81
10/19/09	04.80	04.99	05.30	04.69
10/20/09	05.03	05.23	05.55	04.95
10/21/09	02.42	02.51	02.66	02.39
10/22/09	05.84	06.04	06.40	05.80

10/23/09	05.59	05.77	06.10	05.58
10/24/09	05.96	06.14	06.49	05.98
10/25/09	04.63	04.76	05.02	04.68
10/26/09	02.87	02.95	03.10	02.86
10/27/09	02.45	02.50	02.62	02.39
10/28/09	04.16	04.25	04.43	04.01
10/29/09	01.35	01.37	01.42	01.27
10/30/09	02.84	02.88	02.98	02.64
10/31/09	02.18	02.21	02.28	01.99

Appendix B

FAO CALCULATIONS

Adapted from Allen *et al.* (1998)

Psychrometric Constant

$$\gamma = \frac{C_p P}{\varepsilon \lambda} = 0.665 \times 10^{-3} P \quad (\text{B.1})$$

where:

γ is the psychrometric constant,

P is the atmospheric pressure,

λ is the latent heat of vaporization,

c_p is the specific heat at constant pressure,

and ε is the ratio of the molecular weight of water vapor and dry air.

Slope of the saturated vapor pressure curve

$$\Delta = \frac{4098 \left[0.6108 \exp \left(\frac{17.27T}{T + 237.3} \right) \right]}{(T + 237.3)^2} \quad (\text{B.2})$$

where:

Δ is the slope of saturated vapor pressure curve and
 T is air temperature.

Actual vapor pressure (e_a) from dewpoint temperature (T_{dew}) can be calculated from

$$e_a = 0.6108 \exp \left[\frac{17.27 T_{dew}}{T_{dew} + 237.3} \right] \quad (\text{B.3})$$

Clear-sky solar radiation (R_{so})

$$R_{so} = (a_s + b_s) R_a \quad (\text{B.4})$$

where:

R_{so} is clear-sky solar radiation and

$a_s + b_s$ is the fraction of extraterrestrial radiation reaching the earth on clear-sky days.

Net solar or net shortwave radiation (R_{ns})

$$R_{ns} = (1 - a) R_s \quad (\text{B.5})$$

where:

R_{ns} is net solar or shortwave radiation,

a is the albedo or canopy reflection coefficient and

R_s is the incoming solar radiation

Net longwave radiation (R_{nl})

$$R_{nl} = \sigma \left[\frac{T_{max,K} + T_{min,K}}{2} \right] (0.34 - 0.14 \sqrt{e_a}) \left(1.35 \frac{R_s}{R_{so}} - 0.35 \right) \quad (\text{B.6})$$

where:

R_{nl} net outgoing longwave radiation,

σ is the Stefan-Boltzmann constant,

$T_{max,K}$ and $T_{min,K}$ are the maximum and minimum absolute temperatures during the 24 hour period,

e_a is the actual vapor pressure and

R_s/R_{so} is the relative shortwave radiation.

Net radiation (R_n)

$$R_n = R_{ns} - R_{nl} \quad (\text{B.7})$$